Long-term Particulate Matter Modeling for Health Effects Studies in California – Part II: Concentrations and Sources of Ultrafine Organic Aerosols

Jianlin Hu[1], Shantanu Jathar[2], Hongliang Zhang[3], Qi Ying[4], Shu-Hua Chen[5], Christopher D. Cappa[6], and Michael J. Kleeman[6]**

[1]*Jiangsu Key Laboratory of Atmospheric Environment Monitoring and Pollution Control, Jiangsu Engineering Technology Research Center of Environmental Cleaning Materials, Collaborative Innovation Center of Atmospheric Environment and Equipment Technology, School of Environmental Science and Engineering, Nanjing University of Information Science & Technology, 219 Ningliu Road, Nanjing 210044, China*

[2]*Department of Mechanical Engineering, Colorado State University, Fort Collins CO, USA*

[3]*Department of Civil and Environmental Engineering, Louisiana State University, Baton Rouge LA, USA*

[4]*Zachry Department of Civil Engineering, Texas A&M University, College Station TX, USA*

[5]*Department of Land, Air, and Water Resources, University of California, Davis. One Shields Avenue, Davis, CA, USA*

[6]*Department of Civil and Environmental Engineering, University of California, Davis. One Shields Avenue, Davis CA, USA*

*Corresponding authors:

Jianlin Hu, Tel.: +86 25 5873 1504; E-mail address: jianlinhu@nuist.edu.cn; hu_jianlin@126.com

Michael J. Kleeman, Tel.: +1 530 752 8386; fax; +1 530 752 7872. E-mail address:

mjkleeman@ucdavis.edu

Abstract

Organic aerosol (OA) is a major constituent of ultrafine particulate matter ($PM_{0.1}$). Recent epidemiological studies have identified associations between $PM_{0.1}$ OA and premature mortality and low birth weight. In this study, the source-oriented UCD/CIT model was used to simulate the concentrations and sources of primary organic aerosols (POA) and secondary organic aerosols (SOA) in $PM_{0.1}$ in California for a 9-year (2000 - 2008) modeling period with 4 km horizontal resolution to provide more insights about $PM_{0.1}$ OA for health effects studies. As a related quality control, predicted monthly average concentrations of fine particulate matter ($PM_{2.5}$) total organic carbon at six major urban sites had mean fractional bias of -0.31 to 0.19 and mean fractional errors of 0.4 to 0.59. The predicted ratio of $PM_{2.5}$ SOA/OA was lower than estimates derived from chemical mass balance (CMB) calculations by a factor of 2~3, which suggests the potential effects of processes such as POA volatility, additional SOA formation mechanism, and missing sources. OA in $PM_{0.1}$, the focus size fraction of this study, is dominated by POA. Wood smoke is found to be the single biggest source of $PM_{0.1}$ OA in winter in California, while meat cooking, mobile emissions (gasoline and diesel engines), and other anthropogenic sources (mainly solvent usage and waste disposal) are the most important sources in summer. Biogenic emissions are predicted to be the largest $PM_{0.1}$ SOA source, followed by mobile sources and other anthropogenic sources, but these rankings are sensitive to the SOA model used in the calculation. Air pollution control programs aiming to reduce the $PM_{0.1}$ OA concentrations should consider controlling solvent usage, waste disposal, and mobile emissions in California, but these findings should be revisited after the latest science is incorporated into the SOA exposure calculations. The spatial distributions of SOA associated with different sources are not sensitive to the choice of SOA model, although the absolute amount of SOA can

change significantly. Therefore, the spatial distributions of $PM_{0.1}$ POA and SOA over the 9-year study period provide useful information for epidemiological studies to further investigate the associations with health outcomes.

Key Words: Primary organic aerosols, secondary organic aerosols, California, sources, UCD/CIT model.

1. Introduction

Organic aerosol (OA) is a significant constituent of fine particulate matter ($PM_{2.5}$) (Zhang et al. 2007) and a dominant constituent of ultrafine particulate matter ($PM_{0.1}$) (Kleeman et al. 2009; Sardar et al. 2005b). Epidemiology studies carried out over the past 20 years link $PM_{2.5}$ to severe short-term and long-term health effects such as asthma, cardio-respiratory disease, and lung cancer (Dockery 2001; Dockery and Pope 1994; Dockery et al. 1993; Franklin et al. 2007; Le Tertre et al. 2002; Pope and Dockery 2006; Pope et al. 2002). Epidemiological studies for $PM_{0.1}$ mass are in the early stages of development but preliminary results show associations with premature mortality (Ostro et al. 2015) and low birth weight (Laurent et al. 2014). OA is an important species due to its contribution to $PM_{2.5}$ and $PM_{0.1}$ mass, and the toxicity of some compounds within OA has motivated even greater scrutiny in health studies (Mauderly and Chow 2008). A few $PM_{2.5}$ epidemiology studies have investigated the associations between exposure to OA and health effects with mixed results (Cao et al. 2012; Krall et al. 2013; Levy et al. 2012; Mar et al. 2000; Ostro et al. 2006; Ostro et al. 2010). The early epidemiological studies conducted for $PM_{0.1}$ have identified subcategories of OA that are highly associated with negative health effects (Laurent et al. 2014; Laurent et al. 2016a; Laurent et al. 2016b; Ostro et al. 2015) and these results merit further investigation to identify the exact sources and compound classes that may be related to $PM_{0.1}$ OA toxicity.

The exposure fields used in the published $PM_{0.1}$ epidemiology studies to date have been generated with chemical transport models (CTMs) because $PM_{0.1}$ measurements with sufficient spatial or temporal resolution are not widely available. In these studies, predictions using the UCD/CIT (University of California Davis/California Institute of Technology) model were evaluated against $PM_{2.5}$ and $PM_{0.1}$ point measurements as a confidence building exercise and the

model predictions were then used to estimate exposure fields with ~4km and ~24hr resolution over the state of California (Hu et al. 2014a; Hu et al. 2014b; Hu et al. 2015). The OA exposure fields generated through this approach reflect the state-of-the-science predictions from CTMs at the time they were done, but they may not capture the full complexity of atmospheric OA. OA consists of primary organic aerosol (POA) and secondary organic aerosol (SOA). POA is directly emitted to the atmosphere in the particle phase and SOA is formed in the atmosphere from the oxidation of volatile or semi-volatile organic compounds (Seinfeld and Pankow 2003). Both POA and the precursors of SOA can be emitted from anthropogenic and biogenic sources (Mauderly and Chow 2008). Numerous theories have been put forward about the volatility of POA (Robinson et al. 2007), the conversion of intermediate volatility compounds to SOA (Jathar et al. 2014; Zhao et al. 2014), and the role of water in SOA formation (Jathar et al. 2016; Pankow et al. 2015). A comprehensive model for OA that has been fully constrained by measurements has not been demonstrated to date, which makes it difficult to estimate $PM_{2.5}$ OA exposure using CTMs. However, measurements indicate the OA in the $PM_{0.1}$ size fraction is more heavily influenced by POA (Ham and Kleeman 2011; Kleeman et al. 2009), which makes estimating exposure to $PM_{0.1}$ using CTMs more feasible.

The current paper, as the fourth in the series (Hu et al. 2014a; Hu et al. 2014b; Hu et al. 2015), investigates the UCD/CIT model capability in predicting the concentrations and sources of POA and SOA in $PM_{0.1}$. The objective of this study is to identify the features of the CTM POA and SOA results that could add skill to the exposure assessment for epidemiological studies and to discuss the potential problems in modeling POA and SOA for use in health effects studies.

2. Methods

2.1 Model Description

The source-oriented UCD/CIT air quality model was used to predict OA concentrations in the current study. The UCD/CIT model tracks primary particles and SOA formation from different sources separately through the calculation of all major aerosol processes such as emissions, transport, deposition, gas-to-particle conversion, and coagulation. The standard algorithms of these processes used in the current study are provided in a companion paper (Hu et al. 2015) and references therein, therefore only the details of the algorithms for POA and SOA source apportionment calculation are described here.

The UCD/CIT source-oriented air quality model tracks primary particles emitted from different sources by adding artificial tracers to represent total primary mass contributions from different sources in each particle size bin (Ying et al. 2008). The emissions of tracers are empirically set to be 1% of the total mass of primary particles emitted from each source category, thus the particle radius and the dry deposition rate are not significantly changed. The primary PM total mass concentrations from a given source then are directly correlated with the simulated artificial tracer concentrations from that source. Source specific emission profiles are used to estimate the POA concentrations in the primary PM total mass using the equation (1):

$$POA_{i,j} = C_{i,j} \times A_{i,j} \quad \text{(eq. 1)}$$

where $POA_{i,j}$ and $C_{i,j}$ represent POA concentration and primary PM total mass concentration in size bin *i* from *j*th source, respectively. $A_{i,j}$ represents OA fraction per unit mass of PM emitted from the *j*th emission source in size bin *i*. More details describing the POA source apportionment

technique and the emission profiles are provided in the previous studies (Ying and Kleeman 2004; Ying et al. 2008).

The SOA module used in the current study follows the two-product method described by Carlton et al. (2010). SOA formation is considered from seven precursors: isoprene, monoterpenes, sesquiterpenes, long-chain alkanes, high-yield aromatics, low-yield aromatics, and benzene. The seven precursors form twelve semi-volatile products and seven nonvolatile products. The calculations consider dynamic gas-particle conversion of the semi-volatile and nonvolatile products. A more detailed description of the SOA module and parameters used in gas-to-particle transfer calculation is provided in the part I paper (Hu et al. 2015) and references therein.

The original SOA module described above was modified to have the source apportionment capability inherent in the UCD/CIT model. SOA source apportionment is predicted by tracking the SOA precursor emissions from different sources individually through all atmospheric processes as they react to form low-volatility products that can partition to the particle phase based on the SOA module described above. This approach was initially developed for source apportionment of secondary inorganic aerosols, such as nitrate, sulfate, and ammonium (Mysliwiec and Kleeman 2002; Ying and Kleeman 2006). Later, this approach was applied for SOA source apportionment in California using the Caltech Atmospheric Chemistry Mechanism (Chen et al. 2010; Kleeman et al. 2007) and in Texas using the SAPRC99 mechanism (Zhang and Ying 2011, 2012). In the current study, the SAPRC11 mechanism was used and expanded to track the reactions of SOA precursors emitted from different sources. Chemical reaction products leading to SOA formation are labeled with the source-identity of the

reactant so that source attribution information is preserved. For the example of benzene (BENZ) reaction with OH forming benzene derived SOA,

$$BENZ + OH \rightarrow SV.BNZ1 + SV.BNZ2 \quad \text{(rx. 1)}$$

$$SV.BNZ1 \leftrightarrow ABNZ1 \quad \text{(rx. 2)}$$

$$SV.BNZ2 \leftrightarrow ABNZ2 \quad \text{(rx. 3)}$$

where SV.BNZ1 and SV.BNZ2 represents the two semi-volatile products that partition between gas and particle phase, and ABNZ1 and ABNZ2 represent the particle phase SOA products from SV.BNZ1 and SV.BNZ2, respectively. If there are two sources for BENZ, then BENZ is expanded into two species BENZ_X1 and BENZ_X2 in the model. The above pathways (rx1 – rx3) are then expanded as:

$$BENZ\_X1 + OH \rightarrow SV.BNZ1\_X1 + SV.BNZ2\_X1 \quad \text{(rx. 4)}$$

$$SV.BNZ1\_X1 \leftrightarrow ABNZ1\_X1 \quad \text{(rx. 5)}$$

$$SV.BNZ2\_X1 \leftrightarrow ABNZ2\_X1 \quad \text{(rx. 6)}$$

$$BENZ\_X2 + OH \rightarrow SV.BNZ1\_X2 + SV.BNZ2\_X2 \quad \text{(rx. 7)}$$

$$SV.BNZ1\_X2 \leftrightarrow ABNZ1\_X2 \quad \text{(rx. 8)}$$

$$SV.BNZ2\_X2 \leftrightarrow ABNZ2\_X2 \quad \text{(rx. 9)}$$

Thus, the SOA products from BENZ (i.e., ABNZ1_X1, ABNZ1_X2, ABNZ2_X1 and ABNZ2_X2) contain the information needed to calculate source contributions to the SOA concentrations.

2.2 Model Application

The UCD/CIT model was applied to simulate the concentrations and sources of POA and SOA during ~ a decadal period (9 years from 2000 January 1st to 2008 December 31st) over

California using a one-way nesting technique added to the UCD/CIT model (Zhang and Ying 2010). The parent domain covers the entire state of California using a 24km horizontal grid resolution and two nested domains cover the most populated areas (> 92% of California total population) using a 4km horizontal grid resolution. A detailed description of the emissions inventory used for the analysis has been presented previously (Hu et al. 2015) and so only a brief summary is discussed in the current manuscript. Emissions of the seven SOA precursors were grouped into nine source categories: on-road gasoline engines, off-road gasoline engines, on-road diesel engines, off-road diesel engines, wood smoke, meat cooking, high sulfur fuel combustion, other anthropogenic sources (including solvent usage, waste disposal emissions etc.), and the natural/biogenic sources. Primary PM emissions were also grouped into these 9 source categories. Particulate composition, number and mass concentrations in the range between 0.01 and 10 μm in diameter were represented in 15 size bins with the first 5 bins for $PM_{0.1}$ (0.01 to 0.1 μm) in the model. Biogenic emissions were generated using the U.S. EPA's biogenic emission inventory system (BEIS3.14). Sea salt emissions were estimated based on wind speed as described in the Part I paper (Hu et al. 2015). The Weather Research and Forecasting model (WRF) v3.1.1 (William C. Skamarock June 2008) was used to simulate the 24 km and 4 km hourly meteorological fields (wind, temperature, humidity, precipitation, radiation, air density, and mixing layer height) that drove the UCD/CIT model simulations. WRF simulations were initialized and bounded by the North American Regional Reanalysis (NARR) data with 32 km resolution and 3-hour time resolution. The four-dimensional data assimilation (FDDA) (Liu et al. 2005) technique was used and the surface friction velocity (u*) in the WRF model was increased by 50% to improve the surface wind predictions as suggested by previous studies (Hu et al. 2012; Hu et al. 2010; Mass 2010). Details of the modeling domains, vertical cell spacing, preparation

of emissions and meteorological inputs (including a full comparison to meteorological measurements) are provided in the Part I paper in the series (Hu et al. 2015).

3. Results

3.1 Concentrations of POA and SOA

Hourly POA and SOA concentrations in multiple size fractions were calculated throughout the 9-year simulation period, and then averaged to daily and monthly average concentrations. Although the focus of the current study is $PM_{0.1}$ POA and SOA, the predicted $PM_{2.5}$ OA concentrations were also calculated and compared to measurements as a confidence building exercise (since $PM_{0.1}$ measurements are not routinely available). Model calculations predict organic matter (OM) concentrations while ambient measurements quantify organic carbon (OC) concentrations. Simulated OM concentrations are converted to OC concentrations using an OM/OC ratio of 1.6 for POA (Turpin and Lim 2010) and species-specific OM/OC ratios for SOA species taken from Table 1 in Carlton et al. (2010). Detailed evaluation of the model performance for $PM_{2.5}$ OC (and other PM / gaseous species) has been presented in the first paper in the series (Hu et al. 2015). In summary, predicted monthly average $PM_{2.5}$ OC has a mean fractional bias of -0.32 and a mean fractional error of 0.43. Monthly mean fractional bias (MFB) and mean fractional errors (MFE) (equations E1 and E2 in the Supplemental Materials) calculated using daily average OC generally meet the model performance criteria proposed by Boylan and Russell (2006) (equations E3 and E4 in the Supplemental Materials).

Figure 1 illustrates the time series of the predicted and measured monthly-average total $PM_{2.5}$ OC concentrations at seven major urban locations (a) Sacramento, (b) San Jose, (c) Fresno,

(d) Bakersfield, (e) Los Angeles, (f) Riverside, and (g) El Cajon. At each site, daily average measured concentrations of the $PM_{2.5}$ total mass and OC were obtained from California Air Resources Board (CARB) (CARB 2011) "1 in 3" sampling network and averaged over the 9 year period. Measured $PM_{2.5}$ OC concentrations at all sites show strong seasonal variation with higher concentrations in winter months and lower concentrations in summer months. OC concentrations predicted by the UCD/CIT model generally capture the monthly average concentrations and seasonal variations with MFB ranging from -0.31 to 0.19 and MFE ranging from 0.4 to 0.59. However, the model predicts much weaker trends of $PM_{2.5}$ OC over the 9 years at Los Angeles and Riverside, indicating that the declining emission trends might not be well represented in the inventory. At Sacramento and Fresno, the measured monthly average OC concentrations frequently exceeded 10 $\mu g/m^3$ in winter and the maximum monthly OC concentrations reached or exceeded ~25 $\mu g/m^3$. Wood smoke is predicted to be the dominant OC source in winter at the two locations, contributing over 70% of the total OC concentrations on average. Wood smoke is also predicted to be the dominant OC source in winter at San Jose and Bakersfield. Model calculations tend to over-predict the winter OC concentrations at San Jose, indicating the wood smoke emissions are likely over-estimated in this area. This is consistent with more recent surveys of home heating fuels conducted by the Bay Area Air Quality Management District (BAAQMD). Model calculations generally under-predict OC in summer when concentrations are lower. Meat cooking and other anthropogenic sources are predicted to be the largest sources in summer at Sacramento, San Jose, Fresno, and Bakersfield. Together these two categories contribute over 86% of the total predicted OC in summer. Both measured and predicted seasonal variation is weaker at Los Angeles and Riverside than in Northern California due to smaller wood smoke contributions. Meat cooking and other anthropogenic sources make the largest

predicted contributions to OA at these two Southern California locations. Mobile sources (gasoline and diesel engines) also contribute approximately 30% of the total $PM_{2.5}$ OC at Los Angeles. Model calculations tend to under-predict $PM_{2.5}$ OC concentrations in all seasons in 2000-2006 at Riverside (approximately 80 km downwind of the Los Angeles urban center). Intense emissions transported from the upwind Los Angeles areas along with the meteorology and topography enhances photo-oxidation of volatile organic compounds (VOCs) and formation of SOA at this location. A measurement study of organic aerosols at Riverside in summer indicated high SOA fraction of the total OA with an average SOA/OA ratio of 0.74 (Docherty et al. 2008). The $PM_{2.5}$ OC under-prediction at Riverside during summer and the general under-prediction in summer at other sites may indicate that some important precursors and pathways of $PM_{2.5}$ SOA are missing or only partially included in the current SOA module, such as SOA formation from glyoxal and methylglyoxal (Ervens and Volkamer 2010; Fu et al. 2008; Ying et al. 2015) and from aerosol aqueous phase chemistry (Volkamer et al. 2009), the conversion of intermediate volatility compounds to SOA (Jathar et al. 2014; Zhao et al. 2014), or SOA forming with higher yields than included in the module (Zhang et al., 2014; Cappa et al., 2016).

Figure 2a compares the average $PM_{2.5}$ OC/mass ratios estimated from ambient measurements and the values predicted by the UCD/CIT model over the 9-year study period at seven representative urban locations. Predicted concentrations on the corresponding days were extracted and averaged for the comparison. The average OC/mass ratios were then calculated. The observed average OC/mass ratios vary in the range of 0.24 (at Riverside) to 0.45 (at Sacramento). The predicted average OC/mass ratios are in relatively good agreement with measured values at Los Angeles, Riverside, and Bakersfield (difference < 20%), but not at Sacramento, San Jose, Fresno, and El Cajon (difference > 35%). The predicted average OC/mass

ratios are consistently lower than observed ratios, by 0.01 (3% at Los Angeles) to 0.22 (48% at Sacramento). This under-prediction is partly attributed to the under-prediction of OC concentrations, especially the SOA concentrations, but also to the over-prediction of total mass concentrations due to over-estimated dust emissions (Hu et al. 2014a; Hu et al. 2015). The seasonal average dust emissions used in the current study were not adjusted based on wind speed and soil moisture. A sensitivity analysis was conducted by removing the dust concentrations from the predicted $PM_{2.5}$ mass (Figure 2a). The average predicted OC/mass ratio increased from 0.22 to 0.29 (average across the seven sites), compared to the observed ratio of 0.33. Omission of dust from the model predictions improves agreement with OC/mass measurements at all sites except central Los Angeles, although OC/mass without dust is still lower than measurements at four sites (Sacramento, San Jose, Fresno, and El Cajon) indicating OC predictions are likely biased low at these locations.

Figure 2b compares the predicted and observed OC/mass ratios in the ultrafine ($PM_{0.1}$) or quasi-ultrafine ($PM_{0.18}$, $PM_{0.25}$) particles. The ultrafine/quasi-ultrafine measurement data were compiled in a previous study (Hu et al. 2014a) from published literature (Herner et al. 2005; Kim et al. 2002; Krudysz et al. 2008; Sardar et al. 2005a; Sardar et al. 2005b). The ultrafine or quasi-ultrafine data are more sparse than the $PM_{2.5}$ data, but still cover a sufficient total number of days to allow for robust comparison. The observed OC/mass ratios in ultrafine/quasi-ultrafine sizes vary from 0.43 (at Modesto) to 0.71 (at USC). The predicted ultrafine/quasi-ultrafine OC/mass ratios generally agree well with observed values at all sites. The generally better agreement of OC/mass ratios in the ultrafine/quasi-ultrafine size range compared to the $PM_{2.5}$ size range reflects the fact that SOA formation and dust emissions make limited contributions to ultrafine/quasi-ultrafine concentrations. Condensation of the semi-volatile products to form SOA

mostly takes place in the particle accumulation mode, and is generally not dominant in the ultrafine size range due to the increase in the saturation vapor pressure above small particles (Kelvin effect). Dust components mainly contribute to coarse and fine particles, but make little contribution to the ultrafine particles.

The primary and secondary fraction of total OA cannot be directly measured in ambient OA samples. A few indirect methods have been developed to estimate the POA and SOA concentrations, such as molecular marker-based method (Daher et al. 2011; Daher et al. 2012; Ham and Kleeman 2011; Kleindienst et al. 2007), elemental carbon (EC) tracer method (Cabada et al. 2004; Lim et al. 2003; Polidori et al. 2007; Polidori et al. 2006; Turpin and Huntzicker 1995), water soluble organic carbon content method (Weber et al. 2007), aerosol mass spectrometry factorization method (Aiken et al. 2008; Lanz et al. 2007; Ulbrich et al. 2009), and the un-explained fraction of OA by tracers for major POA categories (Chen et al. 2010; Schauer and Cass 2000). In the current study, $PM_{2.5}$ SOA concentrations were estimated by the molecular marker Chemical Mass Balance (CMB) method (Daher et al. 2012) during sampling periods in 2005-2007 at four locations. $PM_{2.5}$ POA concentrations were then estimated by subtracting $PM_{2.5}$ SOA concentrations estimated by the CMB method from the total measured OA concentrations. Figure 3 shows the $PM_{2.5}$ POA and SOA concentrations predicted by the UCD/CIT model (right dark columns) compared to the $PM_{2.5}$ POA and SOA concentrations estimated using the CMB method (left gray columns). Error bars represent the standard deviation of concentrations estimated during the sampling periods. The total $PM_{2.5}$ OA (i.e., POA + SOA) concentrations predicted by the UCD/CIT model generally agree with measured values (with fractional bias within ±35%) except at the Riverside site (with a fraction bias of -63%). But the $PM_{2.5}$ SOA concentrations predicted by the UCD/CIT model appear to be a factor of 2~3 lower than the

SOA concentrations estimated by the CMB method (ratio ranging from 2.2 at Riverside to 2.8 at WSanG). The $PM_{2.5}$ POA concentrations predicted by the UCD/CIT model are higher than those estimated by the CMB method at WSanG and ESanG1. This may reflect the effects of POA volatility. Studies have indicated that some fraction of POA emissions will evaporate, and this material may undergo photo-oxidation and condense back to particle phase (Robinson et al., 2007). In the current model, POA is treated as non-volatile. Thus, no such evaporation occurs. However, the substantial under-prediction of $PM_{2.5}$ SOA at all sites suggests that some SOA precursors and pathways are likely missing from the current SOA mechanism. Both $PM_{2.5}$ POA and SOA are under-predicted at Riverside, indicating that some important sources are likely missing in that area.

Figure 4 illustrates the predicted total $PM_{0.1}$ OA concentrations (Figure 4a) and the predicted ratios of SOA to total OA averaged over the 9 year modeling period (Figure 4b). High total $PM_{0.1}$ OA concentrations with maximum concentrations > 2 $\mu g/m^3$ are located in urban areas where the POA emissions are large due to human activities. Predicted $PM_{0.1}$ SOA generally accounts for less than 10% of total $PM_{2.5}$ OA at urban areas, but predicted SOA contribute to 10~20% of total OA in suburban areas, and contribute to 20~50% in rural areas. The spatial distribution of $PM_{2.5}$ SOA concentrations and the SOA to total OA ratios (shown in Figure S1) are generally similar to those of $PM_{0.1}$, but $PM_{0.1}$ OA has sharper spatial gradients and the $PM_{0.1}$ SOA fraction is lower than that in $PM_{2.5}$ in urban areas, indicating POA contributes more in the ultrafine size range.

Figure 5 shows the contributions from the 9 precursor species to the $PM_{0.1}$ SOA concentrations (results of $PM_{2.5}$ SOA are shown in Figure S2). Maximum SOA concentrations are located in southern part of the SJV. Monoterpenes, sesquiterpenes, oligomers, and long

alkanes are the most important precursors, contributing over 90% of the total SOA in most areas, while other precursors (xylene, toluene, and benzene) in total contribute less than 10 ng/m^3 to SOA concentrations. These finding are very dependent on the treatment of vapor wall losses during the formulation of the SOA model. The contributions from different precursors to SOA concentrations have very different spatial distributions. Long chain alkanes form SOA mainly in the urban areas of Southern California and in the middle-southern portion of the SJV. Isoprene, monoterpenes, and sesquiterpenes form SOA at coastal and foothill locations where the biogenic emissions are greatest. The longer lifetime of long chain alkanes than isoprene leads to a broader spatial distribution for the SOA derived from alkanes. The spatial distribution of oligomers of anthropogenic SOA (Oligomer_A) and biogenic SOA (Oligomer_B) reflects the patterns of SOA derived from long chain alkanes and the total biogenic species. The relative spatial patterns associated with each precursor are generally not sensitive to the exact formulation of the SOA model (see section 3.3).

3.2 Sources of POA and SOA

Figure 6 displays the time series of monthly average $PM_{0.1}$ SOA source contributions at the six major urban locations. $PM_{0.1}$ SOA concentrations are high in summer (100~300 ng/m^3) and low (20~50 ng/m^3) in winter, reflecting the seasonal variation in photochemistry. $PM_{0.1}$ SOA concentrations are higher at Fresno and Bakersfield than other sites due to larger biogenic source contributions. Biogenic emissions are the largest source of $PM_{0.1}$ SOA across all sites, followed by the other anthropogenic sources (mainly solvent usage and waste disposal emissions, see Figure S3). On-road gasoline engines are an important source of SOA at Los Angeles and

Riverside. Similar source contributions to $PM_{2.5}$ SOA are found and shown in Figure S4 in the Supplemental Materials.

Figure 7 shows the predicted regional source contributions of $PM_{0.1}$ POA averaged over the 9 year modeling period. The important regional sources of $PM_{0.1}$ POA over the entire California are predicted to be other anthropogenic sources (contributing 39.6%), wood smoke (37.1%), on-road gasoline (9.1%), and meat cooking (5.8%). Wood smoke is the dominant POA source especially in Northern California, with the maximum $PM_{0.1}$ POA contribution exceeding 1 $\mu g/m^3$. Meat cooking and mobile (on-road and off-road) sources are the major sources in urban areas, especially in metropolitan areas such as Greater Los Angeles Area and the San Francisco Bay Area. Other anthropogenic sources is another major category in the urban centers in the SJV and also the Los Angeles areas. High sulfur content fuel sources are mainly located around the ports in the Los Angeles and San Francisco Bay areas. The regional source contributions of $PM_{0.1}$ POA are quite different from those of $PM_{2.5}$ POA (shown in Figure S5). The $PM_{2.5}$ POA source contributions are much more widespread than the $PM_{0.1}$ POA sources contributions because $PM_{2.5}$ has a longer lifetime due to slower deposition and coagulation compared to $PM_{0.1}$. For example, the mobile sources and the other anthropogenic sources contribute greatly to $PM_{2.5}$ POA throughout the entire SJV, but only contribute to $PM_{0.1}$ POA in urban centers.

Figure 8 shows the predicted regional source contributions of $PM_{0.1}$ SOA averaged over the 9 year modeling period (and Figure S6 shows the $PM_{2.5}$ SOA results). Biogenic emission is predicted to be the single largest $PM_{0.1}$ SOA source in the present study, contributing 63.7% of the $PM_{0.1}$ SOA over the entire California. The maximum biogenic $PM_{0.1}$ SOA concentration is up to 0.1 $\mu g/m^3$ around Bakersfield in the southern SJV. Other anthropogenic sources (22.2%),

and on-road gasoline engines (10.8%) are predicted to be the most important anthropogenic sources of $PM_{0.1}$ SOA in California. The spatial distribution of $PM_{0.1}$ SOA concentrations from these anthropogenic sources are similar (but different from the spatial distribution of SOA from biogenic sources) with high concentrations in Southern California. $PM_{0.1}$ SOA formation from on-road diesel engines, off-road diesel engines, wood smoke, meat cooking and high sulfur fuel combustion are small, with $PM_{0.1}$ SOA contributions generally less than a few ng/m^3. A recent epidemiological study has revealed that anthropogenic $PM_{0.1}$ SOA is highly associated with ischemic heart disease mortality (Ostro et al. 2015). Therefore, the results in this study suggest that control of solvent usage, waste disposal, and mobile emissions should be considered to protect public health in California, but the exact determination of source controls will need to be evaluated after the SOA formation mechanism is updated.

3.3 Influence of vapor wall losses on SOA exposure in California

The SOA concentrations predicted in the current study are based on the SOA yield data measured in chamber experiments. A recent study has demonstrated that organic vapors can be lost to chamber walls during SOA formation experiments resulting in SOA yields that are biased low (Zhang et al. 2014). Efforts have been carried out to parameterize the effect of vapor wall losses on SOA formation in the UCD/CIT air quality model to account for this effect when predicting ambient SOA concentrations in Southern California (Cappa et al. 2015). SOA concentrations are predicted to increases by factors of 2-5 with low vapor wall loss rates, and by factors of 5-10 with high vapor wall loss rates, compared to the concentrations in the simulations with no consideration of vapor wall losses. Due to low SOA/TOA fractions (< 10%) at the observation sites located in urban areas (Figure 4 and Figure S1), the substantial increase of SOA

by the vapor wall loss corrections does not strongly change the total OA concentrations and therefore does not significantly affect the model evaluation results shown in Figure 1. Here we further analyzed the changes in the population weighted concentrations (PWCs) of SOA when vapor wall losses are accounted for. Two sets of simulations (scenarios) conducted by Cappa et al (2015) are considered, one with the low-NO_x, high-yield parameters (denoted as "highyield") and the other with high-NO_x, low-yield parameters (denoted as "lowyield"). Each set of simulations included three vapor wall loss cases, i.e., no consideration of vapor wall losses (denoted as "base"), low vapor wall loss rates (denoted as "lowwallloss"), and high vapor wall loss rates (denoted as "highwallloss"). PWCs of SOA are calculated for six counties in the Southern California for the six scenarios, respectively. Spatial difference in exposure is important in cohort studies, therefore the relative changes of PWCs among counties are examined. Figure 9 shows the PWCs of SOA and their relative changes in different scenarios in the six counties. The results indicate that PWCs of SOA increase substantially by accounting for vapor wall losses in all counties (panel a). However, the spatial pattern of SOA PWC, as characterized by normalizing the PWC for each location by the PWC in Orange County, is very similar in all scenarios (panel b). Consequently, accounting for vapor wall losses changes the SOA exposure ratio in different counties by only a small extent of < 15% for most scenarios/counties (panel c). These results suggest that future simulations that account for vapor wall losses in SOA simulations will yield increased absolute values of concentrations but will have spatial patterns that are similar to the basecase results in the current paper when used for epidemiology studies.

Figure 9 suggests that associations between anthropogenic SOA and health effects identified in previous epidemiological studies will prove robust to future updates in SOA models. This

finding also extends to the spatial pattern of individual SOA precursors. The influence of vapor wall losses on exposure to SOA formed from different precursors (i.e., long alkanes, aromatics, isoprene, sesquiterpenes, and monoterpenes) is shown in Figures S7-S11. In all cases, the spatial pattern of PWC for SOA derived from each precursor is similar under all treatments of wall losses. Long alkanes and aromatics are mainly from anthropogenic sources, and isoprene, sesquiterpenes, and monoterpenes are mostly from biogenic sources. Further detailed interpretation of source contributions to SOA and associated health effects should only be carried out after new exposure fields are calculated using the latest SOA models.

4. Conclusions

The source-oriented UCD/CIT model was applied to predict the concentrations and sources of $PM_{0.1}$ POA and SOA in California for a 9 year (2000 - 2008) modeling period with 4 km horizontal resolution to provide data for health effects studies. As a confidence building measure, predicted total $PM_{2.5}$ OC concentrations (primary + secondary) and the $PM_{2.5}$ and $PM_{0.1}$ OC/mass ratios generally agree with measured values at fixed point locations. Compared to the POA and SOA concentrations estimated from measurements at 4 sites using the CMB method, the $PM_{2.5}$ total OA concentrations predicted by the UCD/CIT model have a fractional bias within ±35% except at the Riverside site. The CMB model estimated $PM_{2.5}$ SOA concentrations accounted for 13-37% of total OA while the UCD/CIT SOA concentrations accounted for 4-11% of total OA. POA volatility, incomplete SOA formation mechanism, and/or missing sources may account for the discrepancy. For these reasons, the current study focuses on the $PM_{0.1}$ size fraction.

$PM_{0.1}$ OA has larger contributions from primary sources than the $PM_{2.5}$ size fraction. Wood smoke is found to be the single biggest source of $PM_{0.1}$ OA in winter in California, and meat cooking, mobile sources and other anthropogenic sources (mainly solvent usage, and waste disposal) are the most important sources in summer, but these rankings are sensitive to the SOA model used in the calculation. Biogenic emissions are predicted to be the largest $PM_{0.1}$ SOA source, followed by the other anthropogenic sources, and mobile sources. A recent epidemiological study has revealed that anthropogenic $PM_{0.1}$ SOA is highly associated with ischemic heart disease mortality (Ostro et al. 2015). Therefore, the results in the present study suggest that control of solvent usage, waste disposal, and mobile emissions should be considered to protect public health in California, but detailed source control programs can only be carried out after revised calculations are performed using updated SOA models. The predicted spatial distributions of the concentrations and sources of POA and SOA in $PM_{0.1}$ over the 9-year periods provide detailed information for epidemiological studies to further investigate the associations with other health outcomes, and these spatial patterns are generally not sensitive to the treatment of wall losses in the SOA model formulation. All model results included in the current manuscript can be downloaded free of charge at http://faculty.engineering.ucdavis.edu/kleeman/.

Acknowledgement

This study was funded by the United States Environmental Protection Agency under Grant No. R83386401. Although the research described in the article has been funded by the United States Environmental Protection Agency it has not been subject to the Agency's required peer and policy review and therefore does not necessarily reflect the reviews of the Agency and no official endorsement should be inferred.

References

Aiken, A. C., and Coauthors, 2008: O/C and OM/OC Ratios of Primary, Secondary, and Ambient Organic Aerosols with High-Resolution Time-of-Flight Aerosol Mass Spectrometry. *Environ Sci Technol*, **42,** 4478-4485.

Boylan, J. W., and A. G. Russell, 2006: PM and light extinction model performance metrics, goals, and criteria for three-dimensional air quality models. *Atmos Environ*, **40,** 4946-4959.

Cabada, J. C., S. N. Pandis, R. Subramanian, A. L. Robinson, A. Polidori, and B. Turpin, 2004: Estimating the secondary organic aerosol contribution to PM2.5 using the EC tracer method. *Aerosol Science and Technology*, **38,** 140-155.

Cao, J. J., H. M. Xu, Q. Xu, B. H. Chen, and H. D. Kan, 2012: Fine Particulate Matter Constituents and Cardiopulmonary Mortality in a Heavily Polluted Chinese City. *Environ Health Persp*, **120,** 373-378.

Cappa, C. D., S. H. Jathar, M. J. Kleeman, K. S. Docherty, J. L. Jimenez, J. H. Seinfeld, and A. S. Wexler, 2015: Simulating secondary organic aerosol in a regional air quality model using the statistical oxidation model – Part 2: Assessing the influence of vapor wall losses. *Atmospheric Chemistry and Physics Discussion*, **15,** 30081030126.

CARB, 2011: Database: California Air Quality Data - Selected Data Available for Download <http://www.arb.ca.gov/aqd/aqdcd/aqdcddld.htm>. *Accessed in 2011*.

Carlton, A. G., and Coauthors, 2010: Model Representation of Secondary Organic Aerosol in CMAQv4.7. *Environ Sci Technol*, **44,** 8553-8560.

Chen, J. J., Q. Ying, and M. J. Kleeman, 2010: Source apportionment of wintertime secondary organic aerosol during the California regional PM(10)/PM(2.5) air quality study. *Atmos Environ*, **44,** 1331-1340.

Daher, N., and Coauthors, 2011: Chemical Characterization and Source Apportionment of Fine and Coarse Particulate Matter Inside the Refectory of Santa Maria Delle Grazie Church, Home of Leonardo Da Vinci's "Last Supper". *Environ Sci Technol*, **45,** 10344-10353.

Daher, N., and Coauthors, 2012: Characterization, sources and redox activity of fine and coarse particulate matter in Milan, Italy. *Atmos Environ*, **49,** 130-141.

Docherty, K. S., and Coauthors, 2008: Apportionment of Primary and Secondary Organic Aerosols in Southern California during the 2005 Study of Organic Aerosols in Riverside (SOAR-1). *Environ Sci Technol*, **42,** 7655-7662.

Dockery, D. W., 2001: Epidemiologic evidence of cardiovascular effects of particulate air pollution. *Environ Health Persp*, **109,** 483-486.
Dockery, D. W., and C. A. Pope, 1994: Acute Respiratory Effects of Particulate Air-Pollution. *Annual Review of Public Health*, **15,** 107-132.
Dockery, D. W., and Coauthors, 1993: An Association between Air-Pollution and Mortality in 6 United-States Cities. *New Engl J Med*, **329,** 1753-1759.
Ervens, B., and R. Volkamer, 2010: Glyoxal processing by aerosol multiphase chemistry: towards a kinetic modeling framework of secondary organic aerosol formation in aqueous particles. *Atmos Chem Phys*, **10,** 8219-8244.
Franklin, M., A. Zeka, and J. Schwartz, 2007: Association between PM2.5 and all-cause and specific-cause mortality in 27 US communities. *Journal of Exposure Science and Environmental Epidemiology*, **17,** 279-287.
Fu, T. M., D. J. Jacob, F. Wittrock, J. P. Burrows, M. Vrekoussis, and D. K. Henze, 2008: Global budgets of atmospheric glyoxal and methylglyoxal, and implications for formation of secondary organic aerosols. *J Geophys Res-Atmos*, **113**.
Ham, W. A., and M. J. Kleeman, 2011: Size-resolved source apportionment of carbonaceous particulate matter in urban and rural sites in central California. *Atmos Environ*, **45,** 3988-3995.
Herner, J. D., J. Aw, O. Gao, D. P. Chang, and M. J. Kleeman, 2005: Size and composition distribution of airborne particulate matter in northern California: I-particulate mass, carbon, and water-soluble ions. *J Air Waste Manage*, **55,** 30-51.
Hu, J., C. J. Howard, F. Mitloehner, P. G. Green, and M. J. Kleeman, 2012: Mobile Source and Livestock Feed Contributions to Regional Ozone Formation in Central California. *Environ Sci Technol*, **46,** 2781-2789.
Hu, J., H. Zhang, S.-H. Chen, F. Vandenberghe, Q. Ying, and M. J. Kleeman, 2014a: Predicting Primary PM2.5 and PM0.1 Trace Composition for Epidemiological Studies in California. *Environ Sci Technol*, **48,** 4971-4979.
Hu, J., H. Zhang, S. Chen, Q. Ying, F. Vandenberghe, and M. J. Kleeman, 2014b: Identifying PM2.5 and PM0.1 Sources for Epidemiological Studies in California. *Environ Sci Technol*, **48,** 4980-4990.
Hu, J., H. Zhang, Q. Ying, S.-H. Chen, F. Vandenberghe, and M. J. Kleeman, 2015: Long-term particulate matter modeling for health effect studies in California - Part I: model performance on temporal and spatial variations. *Atmos Chem Phys*, **15,** 3445-3461.
Hu, J., Q. Ying, J. J. Chen, A. Mahmud, Z. Zhao, S. H. Chen, and M. J. Kleeman, 2010: Particulate air quality model predictions using prognostic vs. diagnostic meteorology in central California. *Atmos Environ*, **44,** 215-226.

Jathar, S. H., A. Mahmud, K. C. Barsanti, W. E. Asher, J. F. Pankow, and M. J. Kleeman, 2016: Water uptake by organic aerosol and its influence on gas/particle partitioning of secondary organic aerosol in the United States. *Atmos Environ*, **129,** 142-154.

Jathar, S. H., and Coauthors, 2014: Unspeciated organic emissions from combustion sources and their influence on the secondary organic aerosol budget in the United States. *P Natl Acad Sci USA*, **111,** 10473-10478.

Kim, S., S. Shen, C. Sioutas, Y. F. Zhu, and W. C. Hinds, 2002: Size distribution and diurnal and seasonal trends of ultrafine particles in source and receptor sites of the Los Angeles basin. *J Air Waste Manage*, **52,** 297-307.

Kleeman, M. J., Q. Ying, J. Lu, M. J. Mysliwiec, R. J. Griffin, J. J. Chen, and S. Clegg, 2007: Source apportionment of secondary organic aerosol during a severe photochemical smog episode. *Atmos Environ*, **41,** 576-591.

Kleeman, M. J., and Coauthors, 2009: Source Apportionment of Fine (PM1.8) and Ultrafine (PM0.1) Airborne Particulate Matter during a Severe Winter Pollution Episode. *Environ Sci Technol*, **43,** 272-279.

Kleindienst, T. E., M. Jaoui, M. Lewandowski, J. H. Offenberg, C. W. Lewis, P. V. Bhave, and E. O. Edney, 2007: Estimates of the contributions of biogenic and anthropogenic hydrocarbons to secondary organic aerosol at a southeastern US location. *Atmos Environ*, **41,** 8288-8300.

Krall, J. R., G. B. Anderson, F. Dominici, M. L. Bell, and R. D. Peng, 2013: Short-term Exposure to Particulate Matter Constituents and Mortality in a National Study of US Urban Communities. *Environ Health Persp*, **121,** 1148-1153.

Krudysz, M. A., J. R. Froines, P. M. Fine, and C. Sioutas, 2008: Intra-community spatial variation of size-fractionated PM mass, OC, EC, and trace elements in the Long Beach, CA area. *Atmos Environ*, **42,** 5374-5389.

Lanz, V. A., and Coauthors, 2007: Source Attribution of Submicron Organic Aerosols during Wintertime Inversions by Advanced Factor Analysis of Aerosol Mass Spectra. *Environ Sci Technol*, **42,** 214-220.

Laurent, O., J. L. Hu, L. F. Li, M. Cockburn, L. Escobedo, M. J. Kleeman, and J. Wu, 2014: Sources and contents of air pollution affecting term low birth weight in Los Angeles County, California, 2001-2008. *Environ Res*, **134,** 488-495.

Laurent, O., and Coauthors, 2016a: Low birth weight and air pollution in California: Which sources and components drive the risk? *Environ Int*, **92-93,** 471-477.

Laurent, O., and Coauthors, 2016b: A Statewide Nested Case-Control Study of Preterm Birth and Air Pollution by Source and Composition: California, 2001-2008. *Environ Health Persp*, **http://dx.doi.org/10.1289/ehp.1510133**.

Le Tertre, A., and Coauthors, 2002: Short-term effects of particulate air pollution on cardiovascular diseases in eight European cities. *Journal of Epidemiology and Community Health*, **56,** 773-779.
Levy, J. I., D. Diez, Y. P. Dou, C. D. Barr, and F. Dominici, 2012: A Meta-Analysis and Multisite Time-Series Analysis of the Differential Toxicity of Major Fine Particulate Matter Constituents. *American Journal of Epidemiology*, **175,** 1091-1099.
Lim, H. J., B. J. Turpin, L. M. Russell, and T. S. Bates, 2003: Organic and elemental carbon measurements during ACE-Asia suggest a longer atmospheric lifetime for elemental carbon. *Environ Sci Technol*, **37,** 3055-3061.
Liu, Y., A. Bourgeois, T. Warner, S. Swerdlin, and J. Hacker, 2005: An implementation of obs-nudging-based FDDA into WRF for supporting ATEC test operations. *2005 WRF user workshop, Paper 10.7*.
Mar, T. F., G. A. Norris, J. Q. Koenig, and T. V. Larson, 2000: Associations between air pollution and mortality in Phoenix, 1995-1997. *Environ Health Persp*, **108,** 347-353.
Mass, C. F., 2010: University of Washington, Seattle, WA, personal communication.
Mauderly, J. L., and J. C. Chow, 2008: Health effects of organic aerosols. *Inhal Toxicol*, **20,** 257-288.
Mysliwiec, M. J., and M. J. Kleeman, 2002: Source apportionment of secondary airborne particulate matter in a polluted atmosphere. *Environ Sci Technol*, **36,** 5376-5384.
Ostro, B., R. Broadwin, S. Green, W. Y. Feng, and M. Lipsett, 2006: Fine particulate air pollution and mortality in nine California counties: Results from CALFINE. *Environ Health Persp*, **114,** 29-33.
Ostro, B., J. Hu, D. Goldberg, P. Reynolds, A. Hertz, L. Bernstein, and M. J. Kleeman, 2015: Associations of Mortality with Long-Term Exposures to Fine and Ultrafine Particles, Species and Sources: Results from the California Teachers Study Cohort. *Environ Health Persp*, **DOI:10.1289/ehp.1408565**.
Ostro, B., and Coauthors, 2010: Long-Term Exposure to Constituents of Fine Particulate Air Pollution and Mortality: Results from the California Teachers Study. *Environ Health Persp*, **118,** 363-369.
Pankow, J. F., and Coauthors, 2015: Molecular view modeling of atmospheric organic particulate matter: Incorporating molecular structure and co-condensation of water. *Atmos Environ*, **122,** 400-408.
Polidori, A., M. Arhami, C. Sioutas, R. J. Delfino, and R. Allen, 2007: Indoor/Outdoor Relationships, Trends, and Carbonaceous Content of Fine

583 Particulate Matter in Retirement Homes of the Los Angeles Basin. *J Air Waste*
584 *Manage*, **57,** 366-379.
585 Polidori, A., B. J. Turpin, H. J. Lim, J. C. Cabada, R. Subramanian, S. N. Pandis,
586 and A. L. Robinson, 2006: Local and regional secondary organic aerosol:
587 Insights from a year of semi-continuous carbon measurements at Pittsburgh.
588 *Aerosol Science and Technology*, **40,** 861-872.
589 Pope, C. A., and D. W. Dockery, 2006: Health effects of fine particulate air
590 pollution: Lines that connect. *J Air Waste Manage*, **56,** 709-742.
591 Pope, C. A., R. T. Burnett, M. J. Thun, E. E. Calle, D. Krewski, K. Ito, and G. D.
592 Thurston, 2002: Lung cancer, cardiopulmonary mortality, and long-term
593 exposure to fine particulate air pollution. *Jama-Journal of the American*
594 *Medical Association*, **287,** 1132-1141.
595 Robinson, A. L., and Coauthors, 2007: Rethinking Organic Aerosols:
596 Semivolatile Emissions and Photochemical Aging. *Science*, **315,** 1259-1262.
597 Sardar, S. B., P. M. Fine, and C. Sioutas, 2005a: Seasonal and spatial variability
598 of the size-resolved chemical composition of particulate matter (PM10) in the
599 Los Angeles Basin. *J Geophys Res-Atmos*, **110**.
600 Sardar, S. B., P. M. Fine, P. R. Mayo, and C. Sioutas, 2005b: Size-fractionated
601 measurements of ambient ultrafine particle chemical composition in Los
602 Angeles using the NanoMOUDI. *Environ Sci Technol*, **39,** 932-944.
603 Schauer, J. J., and G. R. Cass, 2000: Source apportionment of wintertime gas-
604 phase and particle-phase air pollutants using organic compounds as tracers.
605 *Environ Sci Technol*, **34,** 1821-1832.
606 Seinfeld, J. H., and J. F. Pankow, 2003: Organic atmospheric particulate
607 material. *Annual Review of Physical Chemistry*, **54,** 121-140.
608 Turpin, B. J., and J. J. Huntzicker, 1995: Identification of Secondary Organic
609 Aerosol Episodes and Quantitation of Primary and Secondary Organic Aerosol
610 Concentrations during Scaqs. *Atmos Environ*, **29,** 3527-3544.
611 Turpin, B. J., and H. J. Lim, 2010: Species contributions to PM2.5 mass
612 concentrations: revisiting common assumptions for estimating organic mass.
613 *Aerosol Science and Technology*, **35:1,** 602-610.
614 Ulbrich, I. M., M. R. Canagaratna, Q. Zhang, D. R. Worsnop, and J. L. Jimenez,
615 2009: Interpretation of organic components from Positive Matrix
616 Factorization of aerosol mass spectrometric data. *Atmos Chem Phys*, **9,** 2891-
617 2918.
618 Volkamer, R., P. J. Ziemann, and M. J. Molina, 2009: Secondary Organic Aerosol
619 Formation from Acetylene (C2H2): seed effect on SOA yields due to organic
620 photochemistry in the aerosol aqueous phase. *Atmos. Chem. Phys.*, **9,** 1907-
621 1928.

622 Weber, R. J., and Coauthors, 2007: A study of secondary organic aerosol
623 formation in the anthropogenic-influenced southeastern United States. *J*
624 *Geophys Res-Atmos*, **112**.
625 William C. Skamarock, J. B. K., Jimy Dudhia, David O Gill, Dale M. Barker,
626 Michael G. Duda, Xiang-Yu Huang, Wei Wang, and Jordan G. Powers, June 2008:
627 A Description of the Advanced Research WRF Version 3. *NCAR Technical Note*
628 *NCAR/TN-475+STR*.
629 Ying, Q., and M. J. Kleeman, 2004: Efficient Source Apportionment of Airborne
630 Particulate Matter Using an Internally Mixed Air Quality Model with Artificial
631 Tracers. *Environmental Science and Engineering (China)*, **1,** 91-99.
632 Ying, Q., and M. J. Kleeman, 2006: Source contributions to the regional
633 distribution of secondary particulate matter in California. *Atmos Environ*, **40,**
634 736-752.
635 Ying, Q., J. Li, and S. H. Kota, 2015: Significant Contributions of Isoprene to
636 Summertime Secondary Organic Aerosol in Eastern United States. *Environ Sci*
637 *Technol*, **49,** 7834-7842.
638 Ying, Q., J. Lu, A. Kaduwela, and M. Kleeman, 2008: Modeling air quality during
639 the California Regional PM10/PM2.5 Air Quality Study (CPRAQS) using the
640 UCD/CIT Source Oriented Air Quality Model - Part II. Regional source
641 apportionment of primary airborne particulate matter. *Atmos Environ*, **42,**
642 8967-8978.
643 Zhang, H., and Q. Ying, 2011: Secondary organic aerosol formation and source
644 apportionment in Southeast Texas. *Atmos Environ*, **45,** 3217-3227.
645 ——, 2012: Secondary organic aerosol from polycyclic aromatic hydrocarbons
646 in Southeast Texas. *Atmos Environ*, **55,** 279-287.
647 Zhang, H. L., and Q. Ying, 2010: Source apportionment of airborne particulate
648 matter in Southeast Texas using a source-oriented 3D air quality model. *Atmos*
649 *Environ*, **44,** 3547-3557.
650 Zhang, Q., and Coauthors, 2007: Ubiquity and dominance of oxygenated
651 species in organic aerosols in anthropogenically-influenced Northern
652 Hemisphere midlatitudes. *Geophysical Research Letters*, **34,** L13801.
653 Zhang, X., C. D. Cappa, S. H. Jathar, R. C. Mcvay, J. J. Ensberg, M. J. Kleeman, and J.
654 H. Seinfeld, 2014: Influence of vapor wall loss in laboratory chambers on
655 yields of secondary organic aerosol. *P Natl Acad Sci USA*, **111,** 5802-5807.
656 Zhao, Y. L., and Coauthors, 2014: Intermediate-Volatility Organic Compounds:
657 A Large Source of Secondary Organic Aerosol. *Environ Sci Technol*, **48,** 13743-
658 13750.

659

660 Figures and Tables

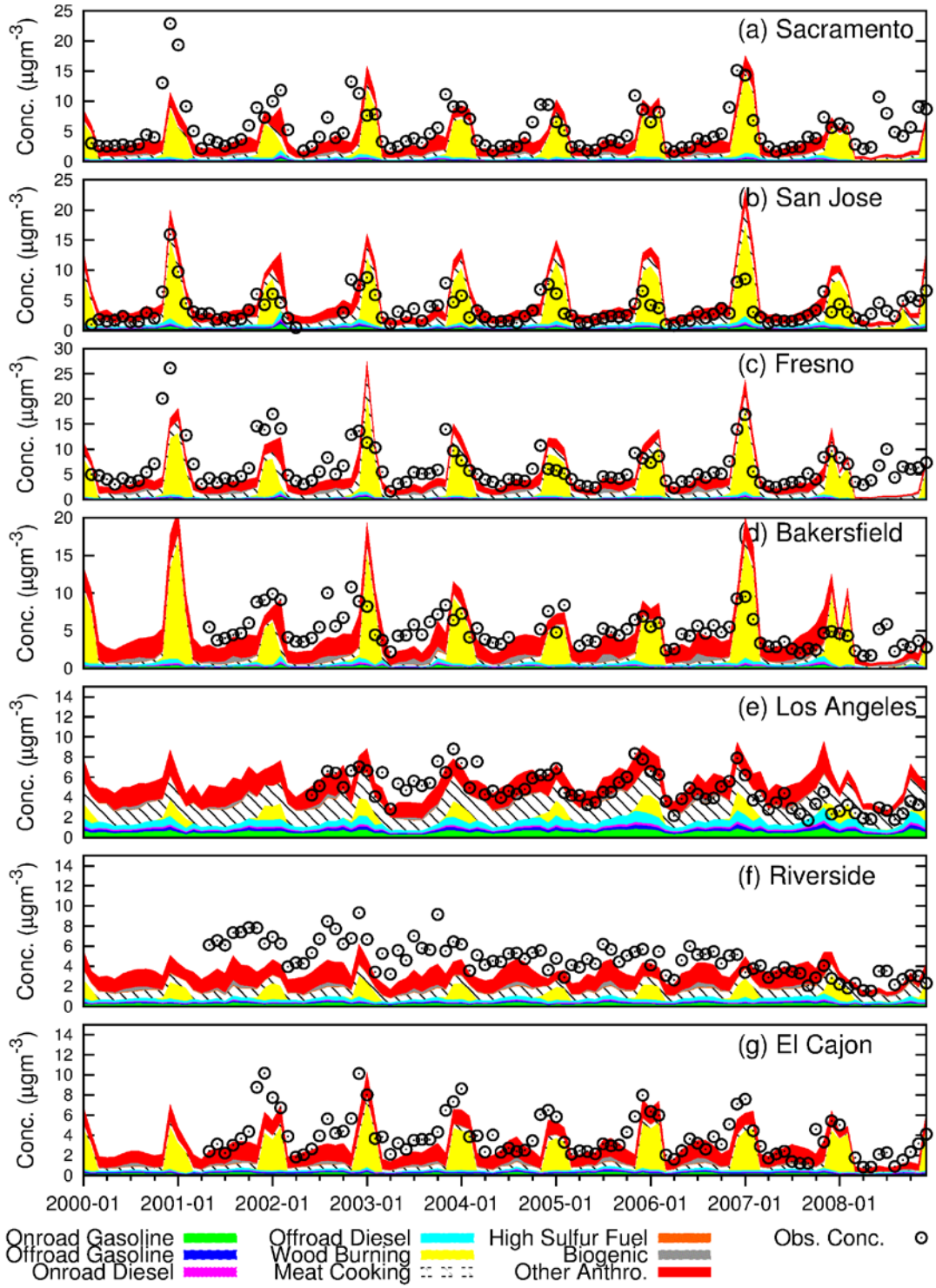

661

662 Figure 1. Monthly source contributions to $PM_{2.5}$ total OC at 7 urban sites. Observed total OC
663 concentrations are indicated by the dot-circles, and predicted OC concentrations from different
664 sources are indicated by the colored areas.

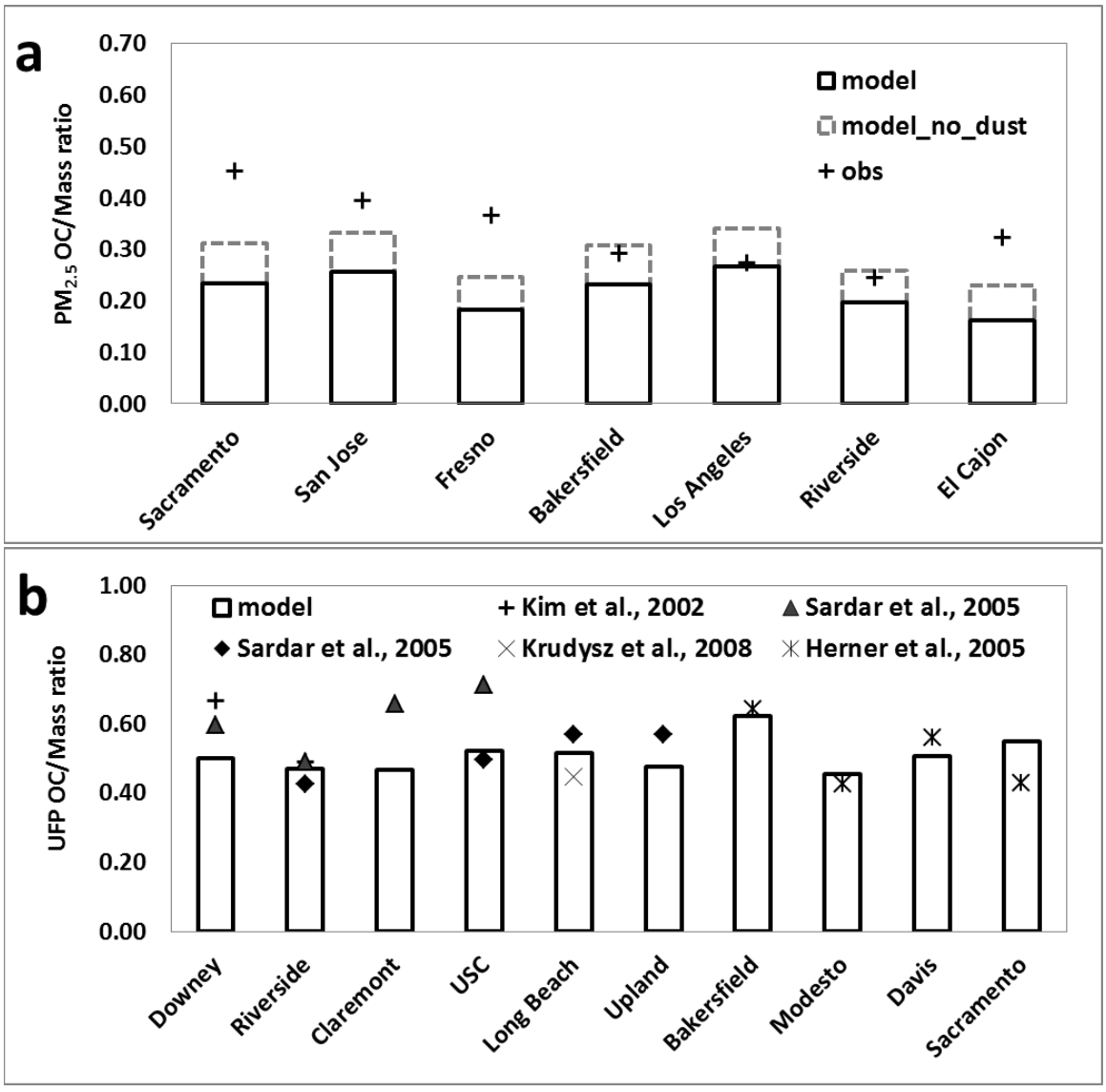

Figure 2. Observed (obs) and predicted (model) OC/Mass ratios in (a) $PM_{2.5}$ and (b) ultrafine and quasi-ultrafine PM. In (a), a sensitivity analysis is conducted by removing the dust concentration from the $PM_{2.5}$ total mass (model_no_dust).The ultrafine and quasi-ultrafine data in (b) are extracted from published literature as indicated in the figure.

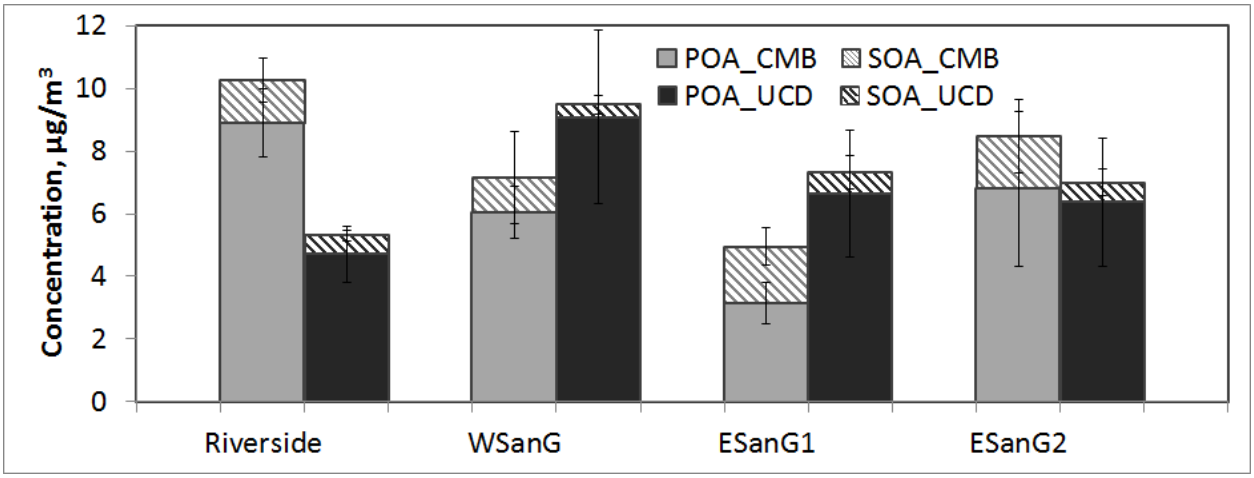

Figure 3. POA and SOA concentrations estimated by the CMB method (left gray columns) and predicted by the UCD/CIT model (right dark columns). Error bars represent the standard deviation of concentrations estimated during the sampling periods by both methods. The uncertainties of CMB derived SOA range from 1% - 22% (Daher et al., 2012). The data are for sampling periods in 2005-2007 at four sites in Southern California.

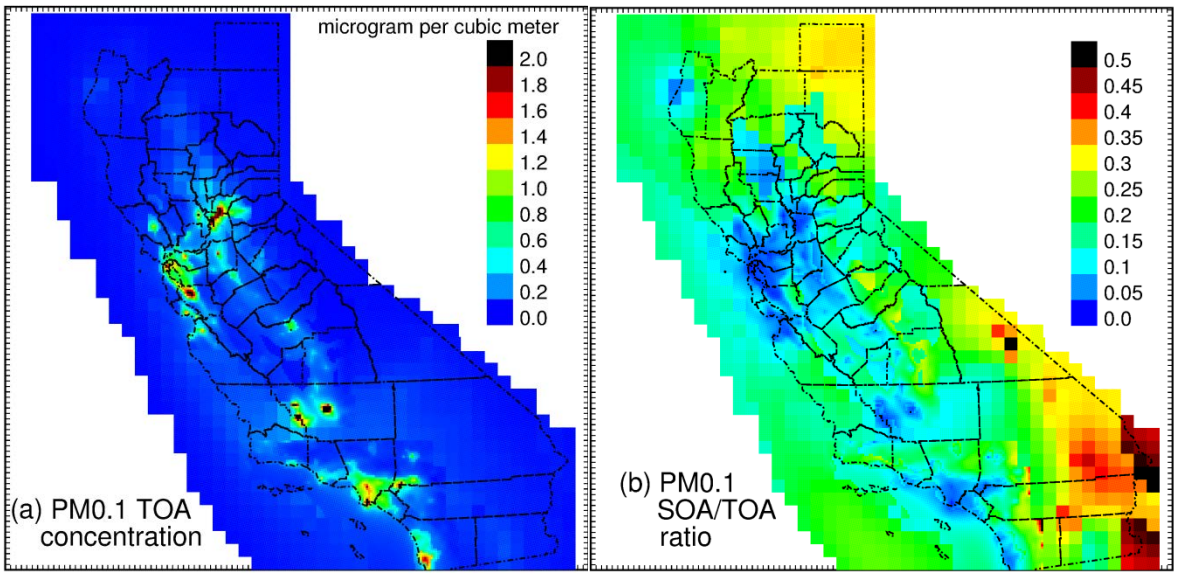

Figure 4. Predicted 9-year average (a) $PM_{0.1}$ Total OA (TOA) concentration and (b) $PM_{0.1}$ SOA/TOA ratio in California.

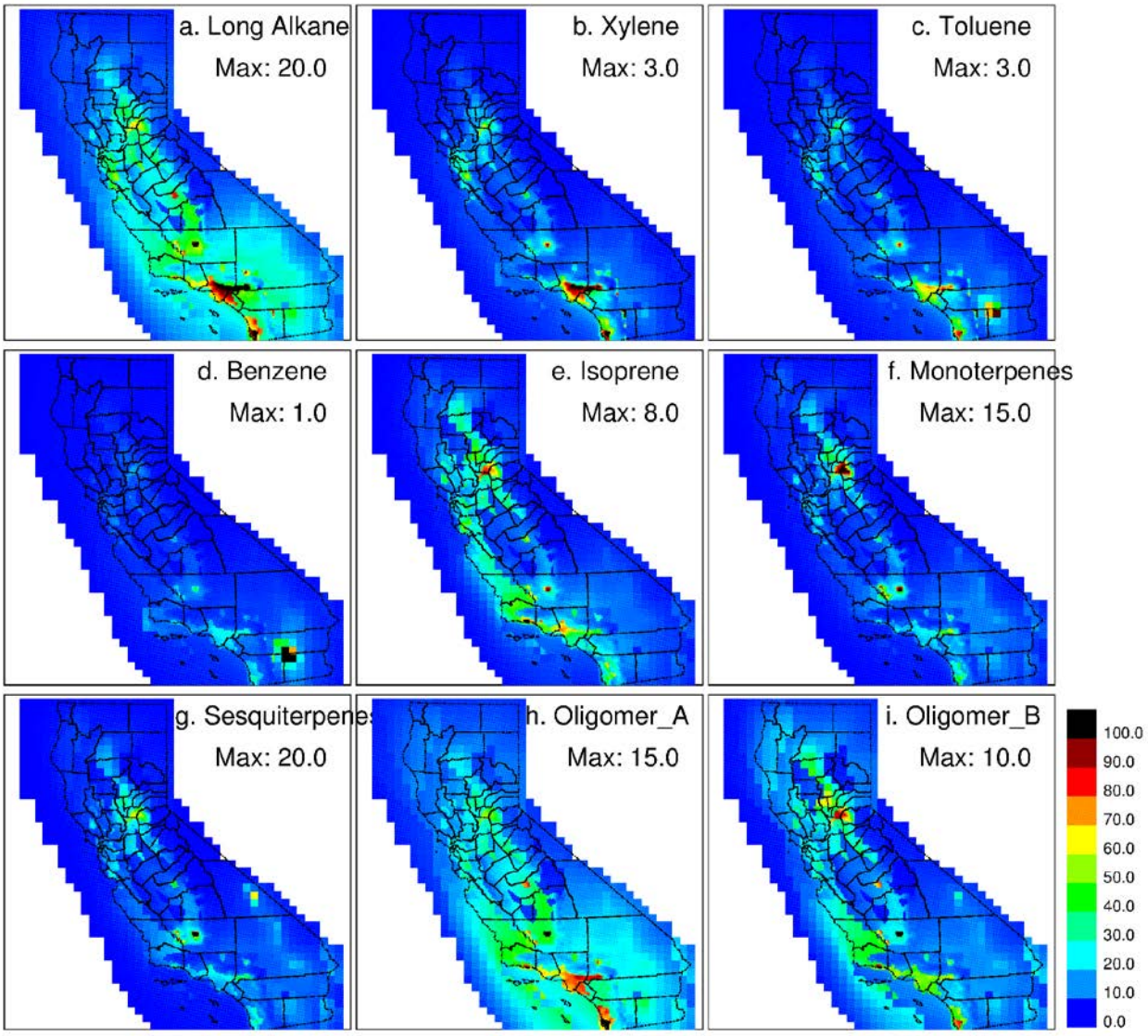

Figure 5. The 9-year average $PM_{0.1}$ SOA concentrations derived from (a) AALK, b) AXYL, c) ATOL, d) ABNZ, e) AISO, f) ATRP, g) ASQT, h) AOLGA, and i) AOLGB. Note AXYL and ATOL are actually derived from lumped aromatics species ARO2 (groups of aromatics with kOH > 2×10^4 ppm^{-1} min^{-1}, including xylenes and other di- and polyalkylbenzenes) and ARO1 (groups of aromatics with kOH < $\times10^4$ ppm^{-1} min^{-1}, including toluene and monoalkylbenzenes). The color scales (shown in the last panel in unit of %) indicate the ratios of the concentrations to the maximum 9-year average values, which are shown in the panels under species names with a unit of ng/m^3.

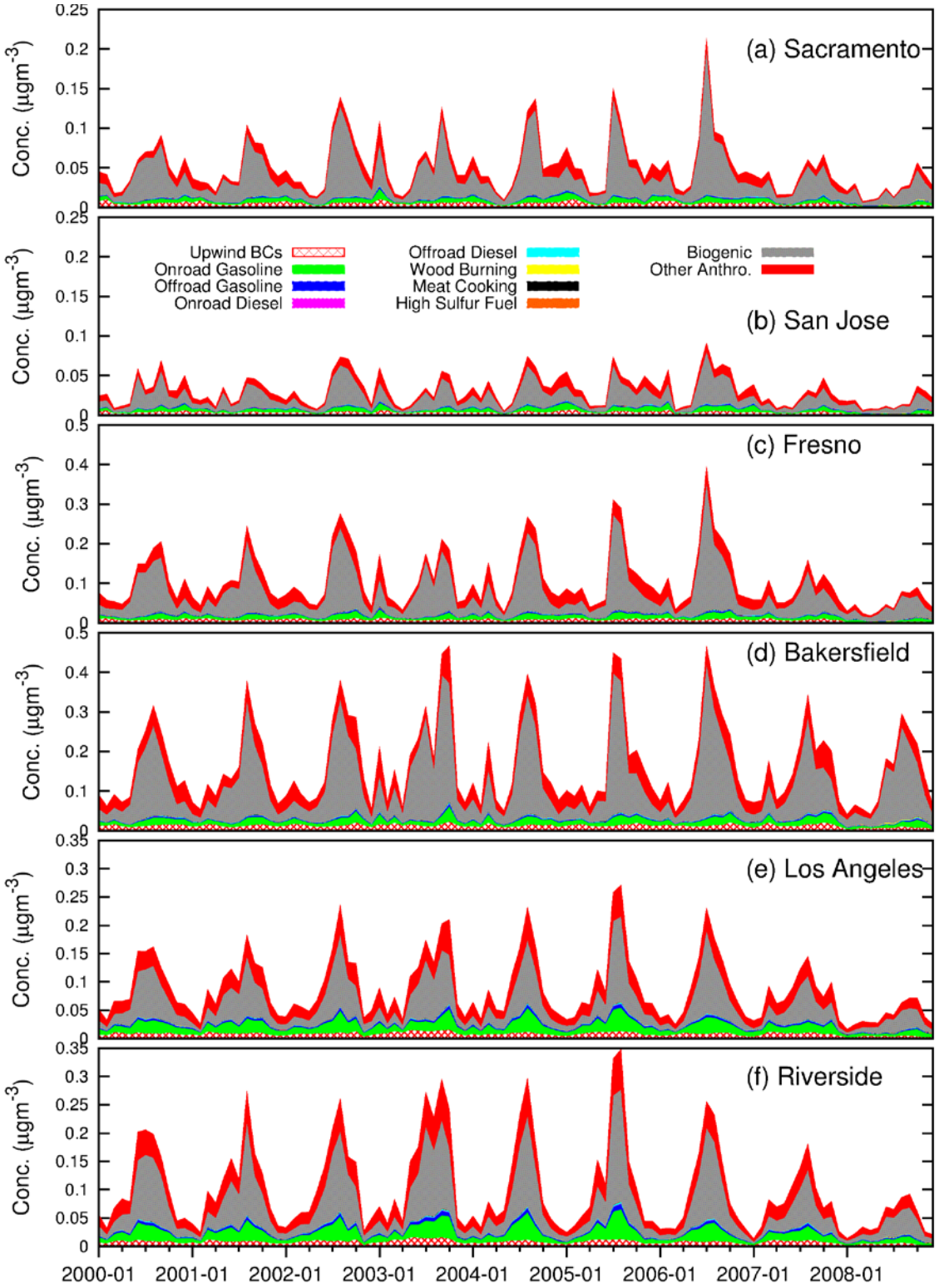

692

693 Figure 6. Monthly source contributions to $PM_{0.1}$ SOA at 6 urban sites. Predicted $PM_{0.1}$ SOA
694 concentrations from different sources are indicated by the colored areas.

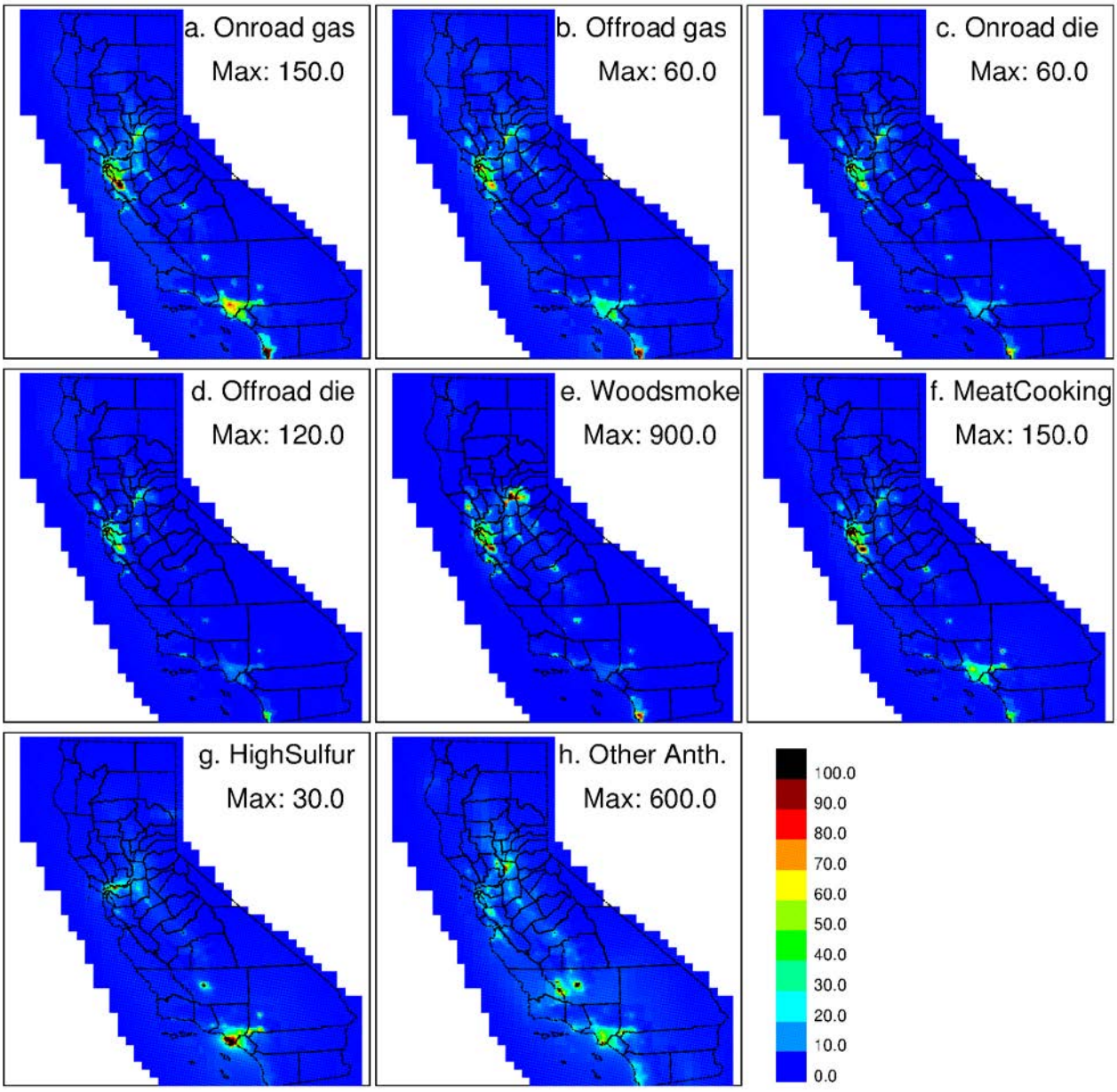

695

696 Figure 7. Predicted source contributions to 9-year average $PM_{0.1}$ POA concentrations. The color
697 scales (shown in the last panel in unit of %) indicate the ratio of the concentrations to the
698 maximum 9-year average concentration values, which are shown in the panels under source
699 names with a unit of ng/m^3.

700

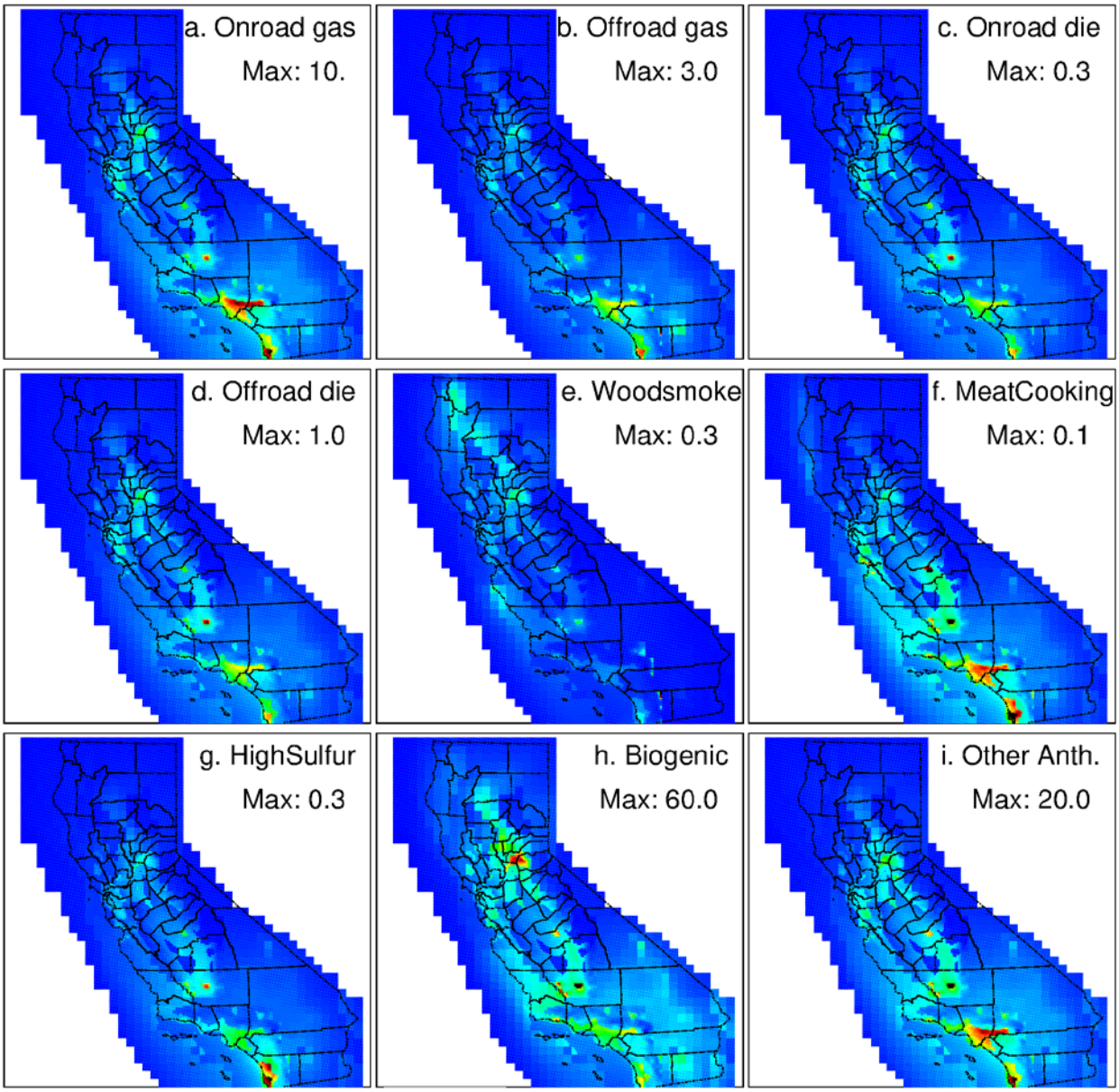

Figure 8. Predicted source contributions to 9-year average $PM_{0.1}$ SOA concentrations. The definition of the color scales are the same as in Figure 7.

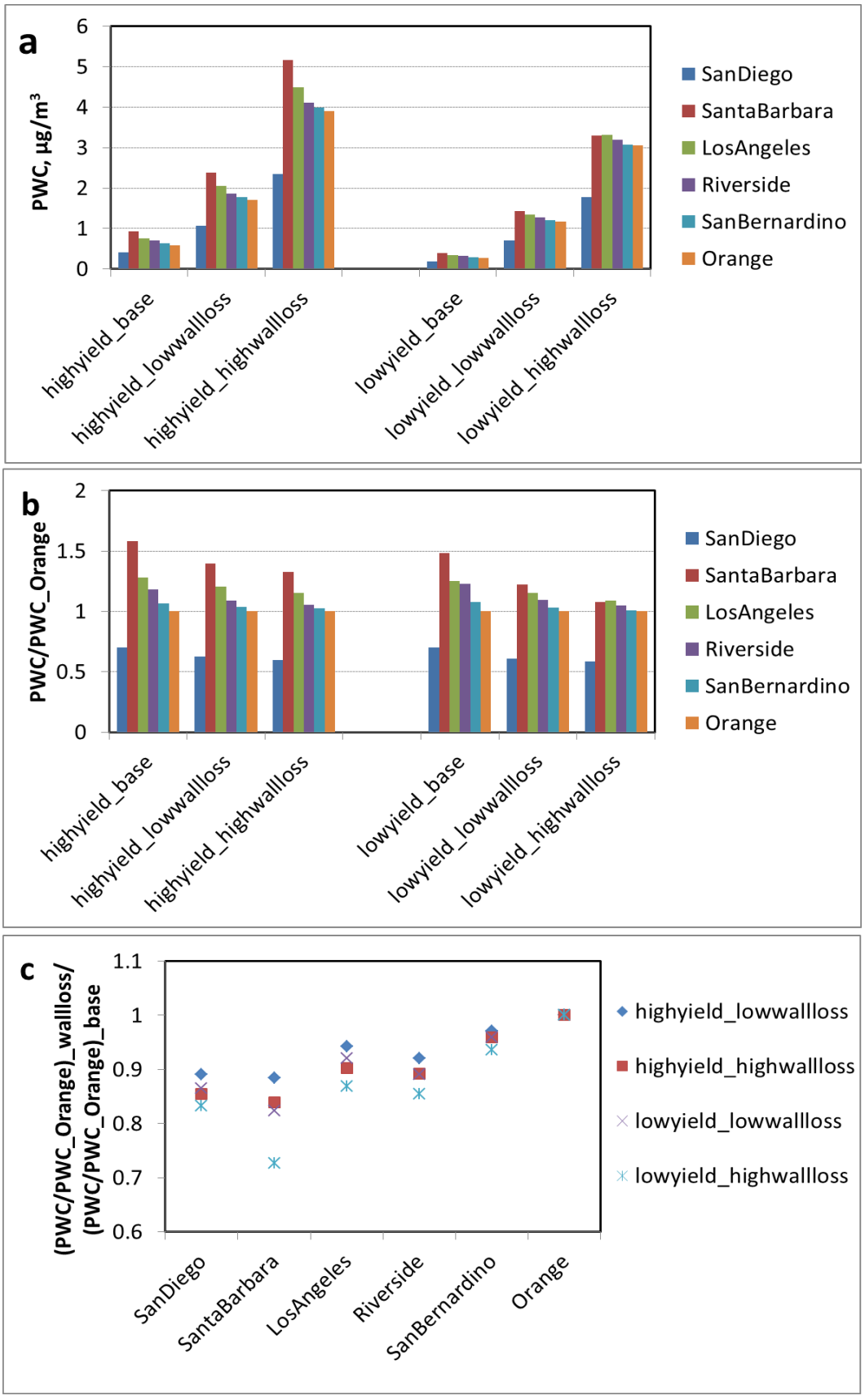
a
PWC, µg/m³
6
5
4
3
2
1
0
highyield_base
highyield_lowwallloss
highyield_highwallloss
lowyield_base
lowyield_lowwallloss
lowyield_highwallloss
SanDiego
SantaBarbara
LosAngeles
Riverside
SanBernardino
Orange
b
PWC/PWC_Orange
2
1.5
1
0.5
0
highyield_base
highyield_lowwallloss
highyield_highwallloss
lowyield_base
lowyield_lowwallloss
lowyield_highwallloss
SanDiego
SantaBarbara
LosAngeles
Riverside
SanBernardino
Orange
c
(PWC/PWC_Orange)_wallloss/
(PWC/PWC_Orange)_base
1.1
1
0.9
0.8
0.7
0.6
SanDiego
SantaBarbara
LosAngeles
Riverside
SanBernardino
Orange
highyield_lowwallloss
highyield_highwallloss
lowyield_lowwallloss
lowyield_highwallloss

705

Figure 9. (a) Predicted population weighted concentrations (PWCs) of SOA in six counties in Southern California. Two sets of simulations (scenarios) conducted by Cappa et al (2015) were used, one with the low-NO_x, high-yield parameters (denoted as "highyield") and the other with high-NO_x, low-yield parameters (denoted as "lowyield"), and each set of simulations included three vapor wall loss cases, i.e., no considering of vapor wall losses (denoted as "base"), low vapor wall loss rates (denoted as "lowwallloss"), and high vapor wall loss rates (denoted as "highwallloss"). (b) Normalized PWCs of SOA in all counties to the PWC of SOA in Orange County. (c) Changes in the normalized PWCs of SOA in all counties by accounting for vapor wall losses.

Long-term Particulate Matter Modeling for Health Effects Studies in California – Part II: Concentrations and Sources of Ultrafine Organic Aerosols

Jianlin Hu[1], Shantanu Jathar[2], Hongliang Zhang[3], Qi Ying[4], Shu-Hua Chen[5], Christopher D. Cappa[6], and Michael J. Kleeman[6]**

[1]*Jiangsu Key Laboratory of Atmospheric Environment Monitoring and Pollution Control, Jiangsu Engineering Technology Research Center of Environmental Cleaning Materials, Collaborative Innovation Center of Atmospheric Environment and Equipment Technology, School of Environmental Science and Engineering, Nanjing University of Information Science & Technology, 219 Ningliu Road, Nanjing 210044, China*

[2]*Department of Mechanical Engineering, Colorado State University, Fort Collins CO, USA*

[3]*Department of Civil and Environmental Engineering, Louisiana State University, Baton Rouge LA, USA*

[4]*Zachry Department of Civil Engineering, Texas A&M University, College Station TX, USA*

[5]*Department of Land, Air, and Water Resources, University of California, Davis. One Shields Avenue, Davis, CA, USA*

[6]*Department of Civil and Environmental Engineering, University of California, Davis. One Shields Avenue, Davis CA, USA*

*Corresponding authors:

Jianlin Hu, Tel.: +86 25 5873 1504; E-mail address: jianlinhu@nuist.edu.cn; hu_jianlin@126.com

Michael J. Kleeman, Tel.: +1 530 752 8386; fax; +1 530 752 7872. E-mail address: mjkleeman@ucdavis.edu

715

716 **Supplemental Mateirals**

717

718 Equations:

719 MFB and MFE are calculated using equation E1 and E2, respectively.

720
$$MFB = \frac{1}{N}\sum_{i=1}^{N}\frac{\left(C_m - C_o\right)}{\left(\frac{C_o + C_m}{2}\right)} \quad \text{(E1)}$$

721
$$MFE = \frac{1}{N}\sum_{i=1}^{N}\frac{\left|C_m - C_o\right|}{\left(\frac{C_o + C_m}{2}\right)} \quad \text{(E2)}$$

722 The PM model performance criteria of MFB and MFE, suggested by Boylan and Russell (2006),
723 are a function of PM concentration as follows:

724
$$\text{MFB (\%)} \leqslant \pm 140 e^{-(Co+Cm)} + 60 \quad \text{(E3)}$$

725
$$\text{MFE (\%)} \leqslant 125 e^{-2(Co+Cm)/3} + 75 \quad \text{(E4)}$$

726 Where Co and Cm in E1-E4 represent the observed and predicted PM concentrations,
727 respectively.

728

729 Tables and Figures:

730 Figure S1: Predicted 9 year average $PM_{2.5}$ Total OA concentration and SOA/TOA ratio in
731 California

732 Figure S2: $PM_{2.5}$ SOA concentrations formed from different precursors.

733 Figure S3: Emission of different sources of long alkanes and aromatics in the "other
734 anthropogenic" source category.

735 Figure S4: Monthly source contributions to $PM_{2.5}$ SOA at 6 urban sites.

736 Figure S5: Predicted source contributions to 9 year average $PM_{2.5}$ POA concentrations.

737 Figure S6: Predicted source contributions to 9 year average $PM_{2.5}$ SOA concentrations.

738 Figure S7-S11: Influence of accounting for vapor wall losses on SOA results for SOA derived
739 from long alkanes (S1), aromatics (S2), isoprene (S3), sesquiterpenes (S4), and monoterpenes
740 (S5).

741

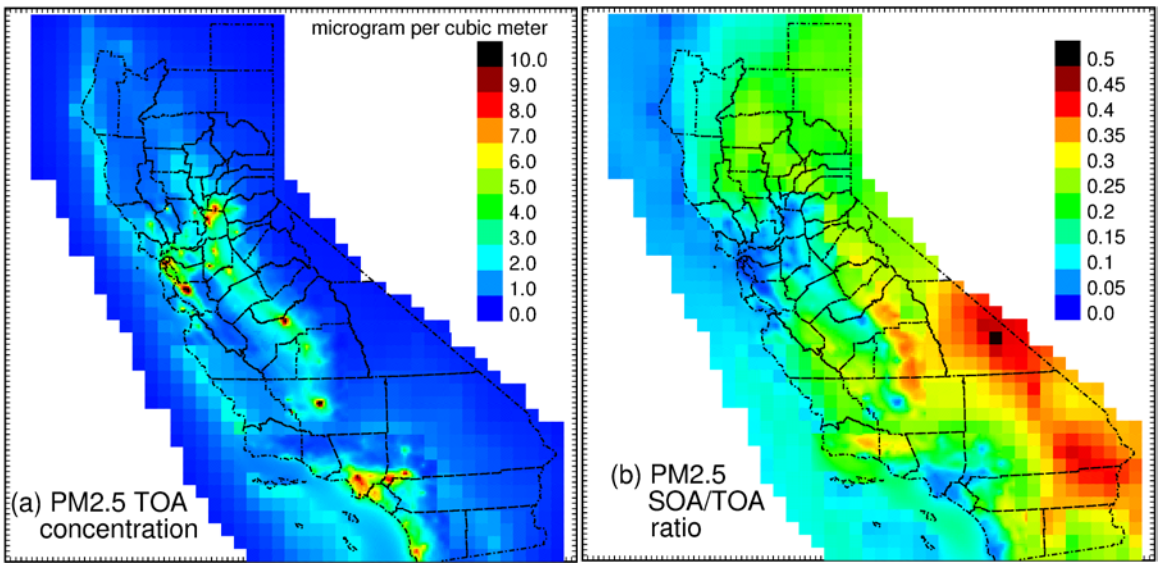

742

743 Figure S1. Predicted 9-year average (a) $PM_{2.5}$ Total OA (TOA) concentrations and (b) $PM_{2.5}$
744 SOA/TOA ratios in California. Natural sources including windblown dust contribute more to the
745 $PM_{2.5}$ size fraction than the $PM_{0.1}$ size fraction in remote regions at the northeast and southeast
746 corners of the state, which explains the different behavior illustrated in Figure 4 and Figure S1.

747

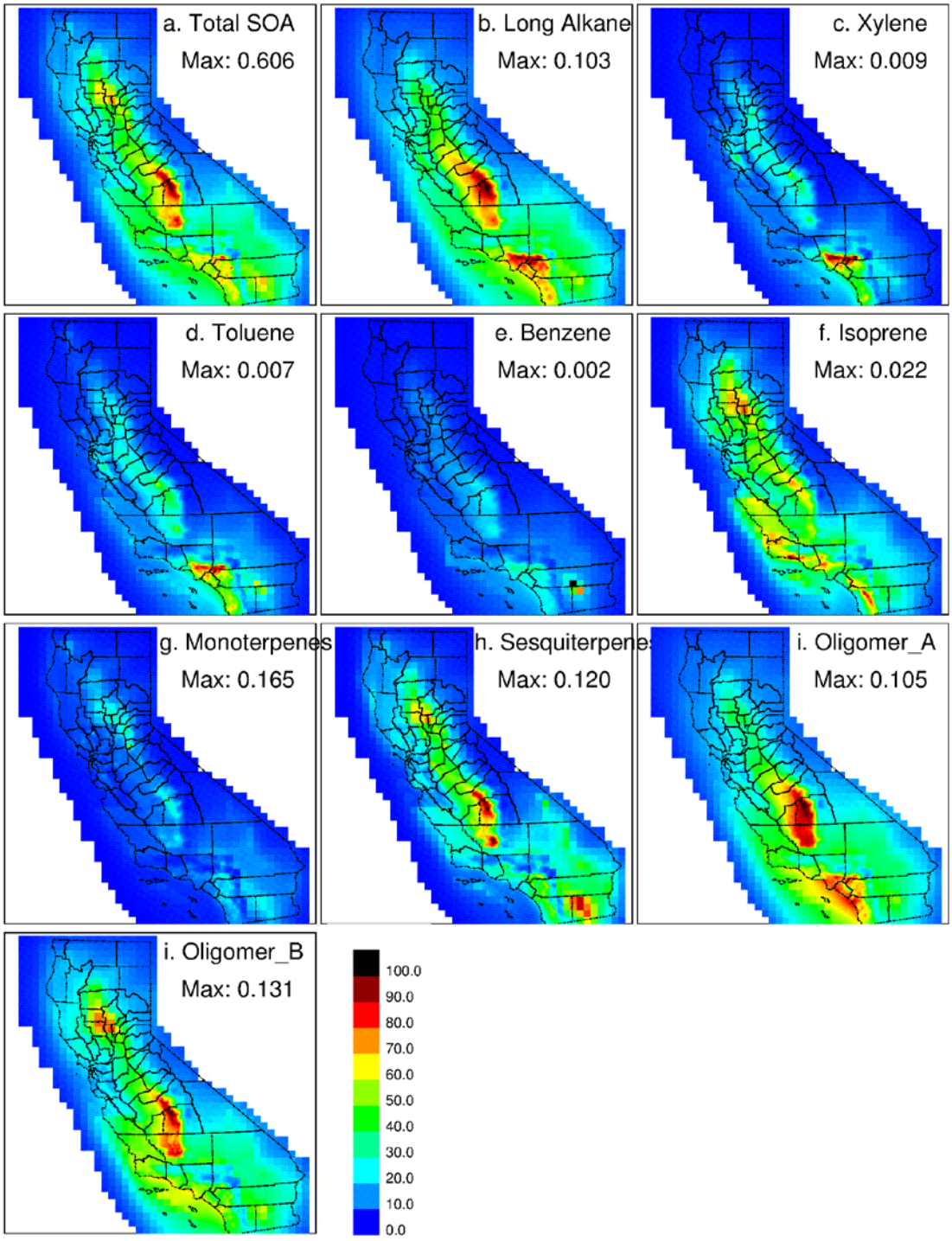

Figure S2. (a) 9-year average SOA concentrations; and SOA formed from (b)AALK, (c) AXYL, (d) ATOL, (e) ABNZ, (f) AISO, (g) ATRP, (h) ASQT, (i) AOLGA, and (j) AOLGB in $PM_{2.5}$. The color scales (shown in the last panel in unit of %) indicate the ratio of the concentrations to the max concentration values. The maximum concentration values are shown in the panels under the names of the species, with a unit of $\mu g/m^3$.

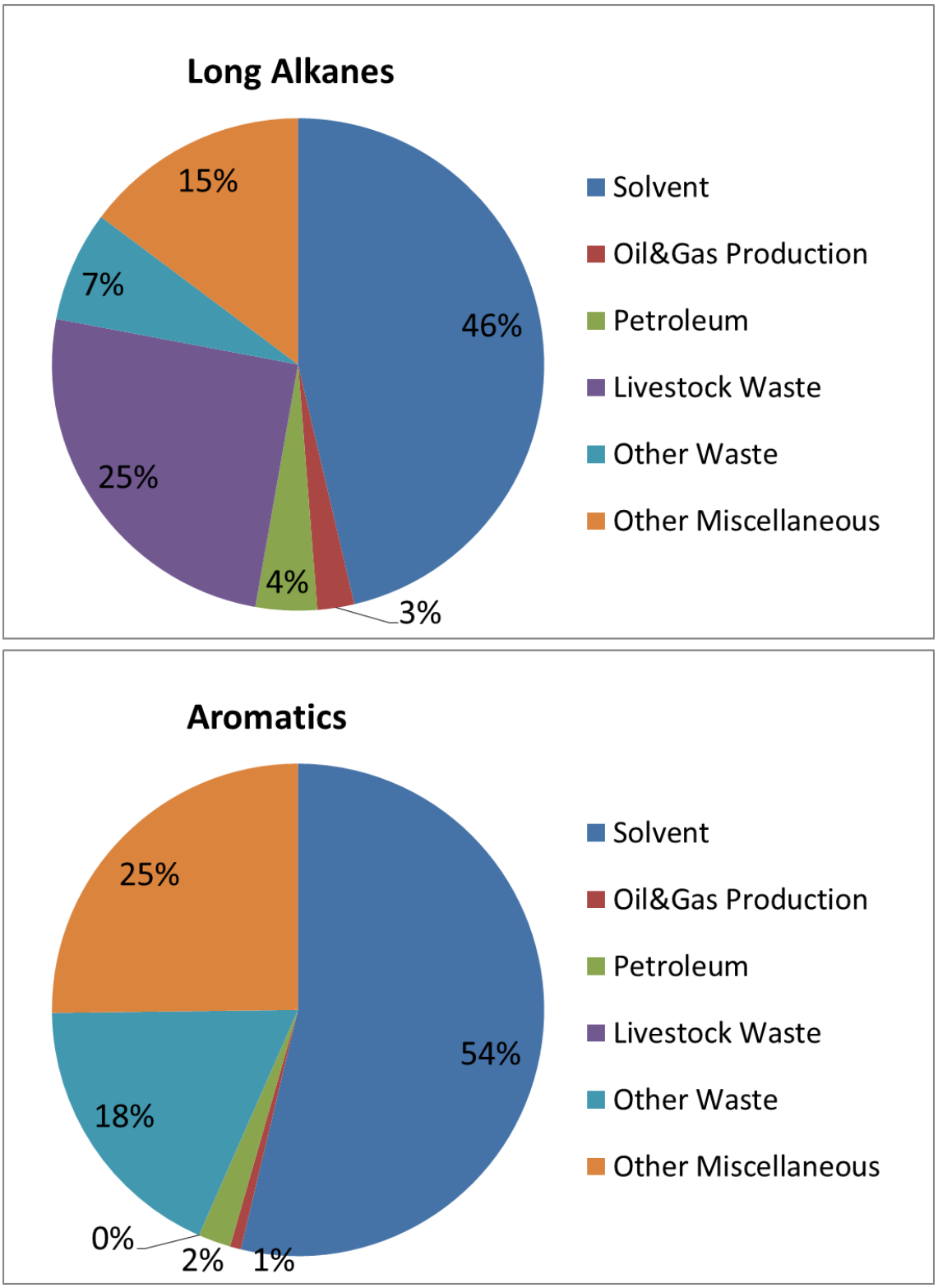

754

755 Figure S3. Emission of different sources of long alkanes and aromatics in the "other
756 anthropogenic" source category.

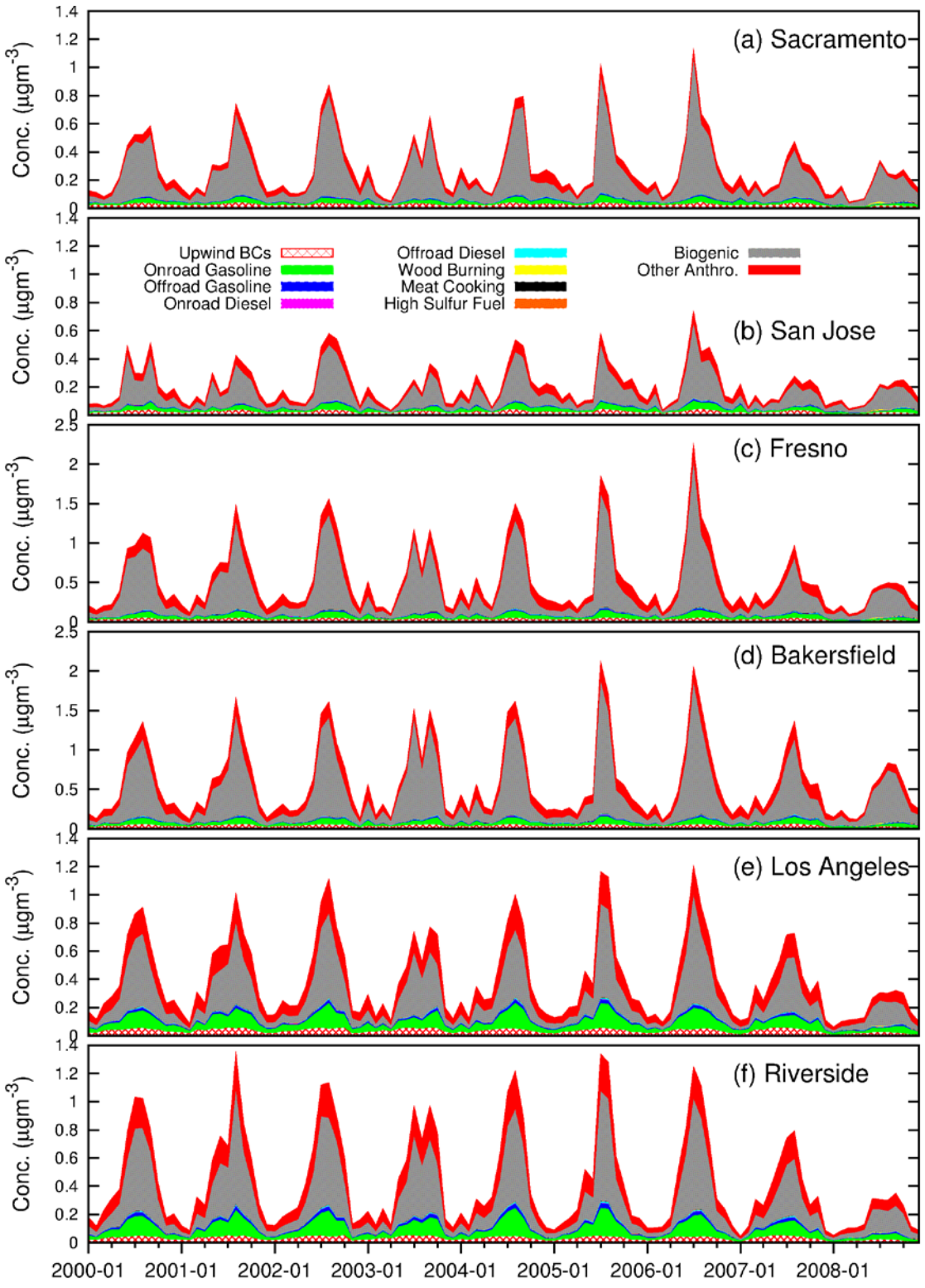

Figure S4. Monthly source contributions to $PM_{2.5}$ SOA at 6 urban sites. Predicted SOA concentrations from different sources are indicated by the colored areas.

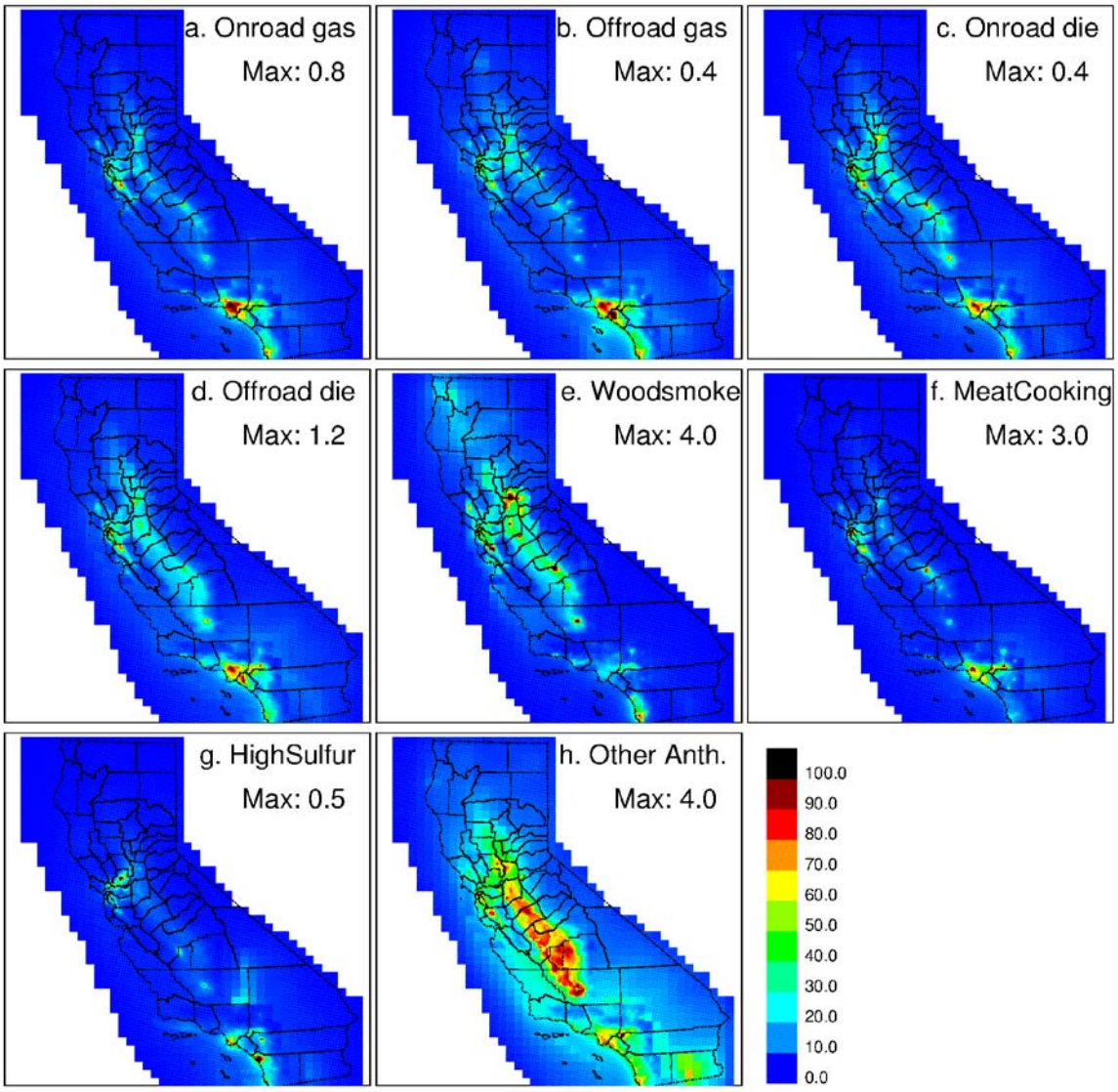

760

761 Figure S5. Predicted source contributions to 9 year average $PM_{2.5}$ POA concentrations. The
762 definition of the color scales are the same as in Figure 5.

763

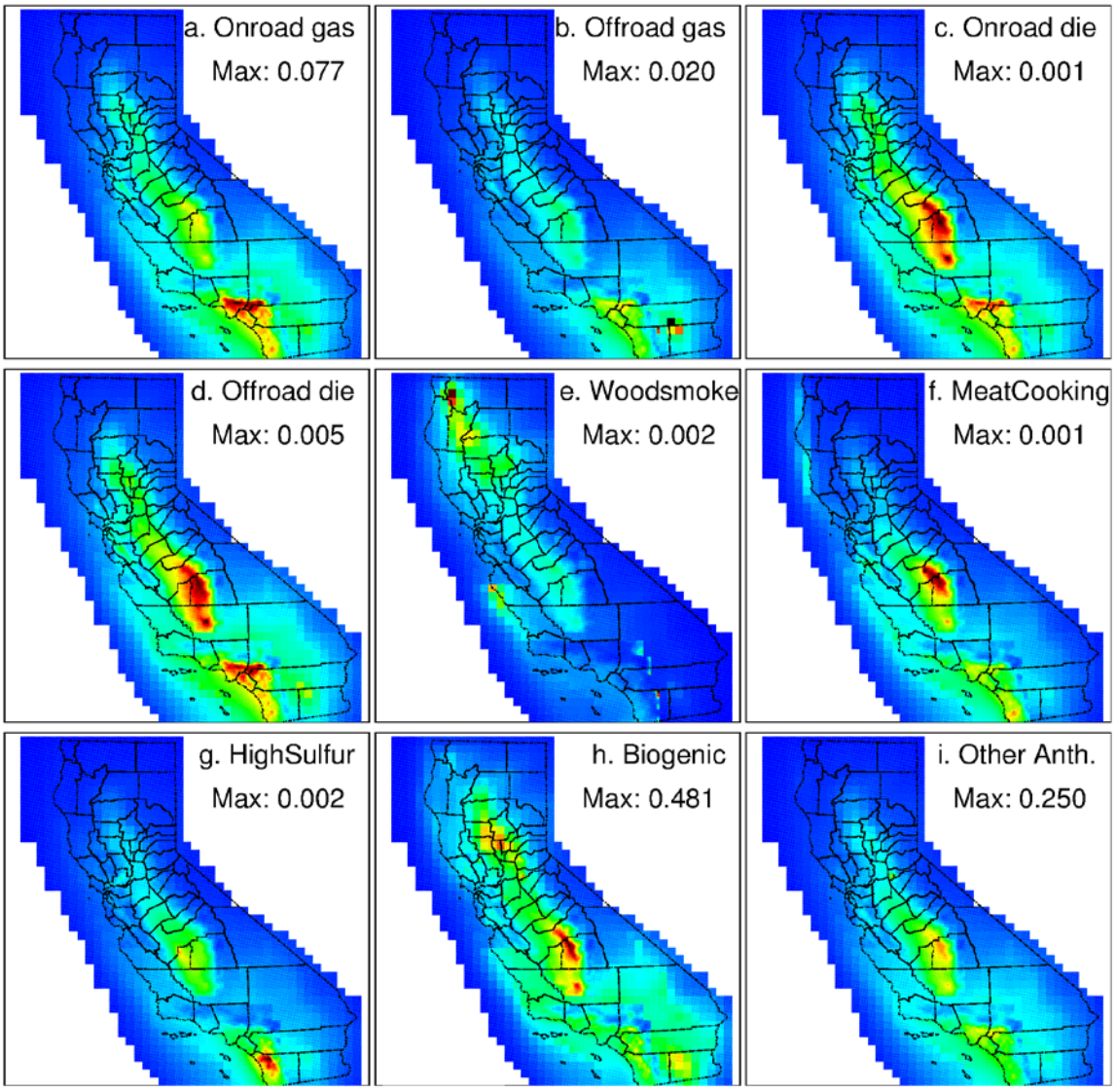

764

765 Figure S6. Predicted source contributions to 9 year average $PM_{2.5}$ SOA concentrations. The
766 definition of the color scales are the same as in Figure 5.

767

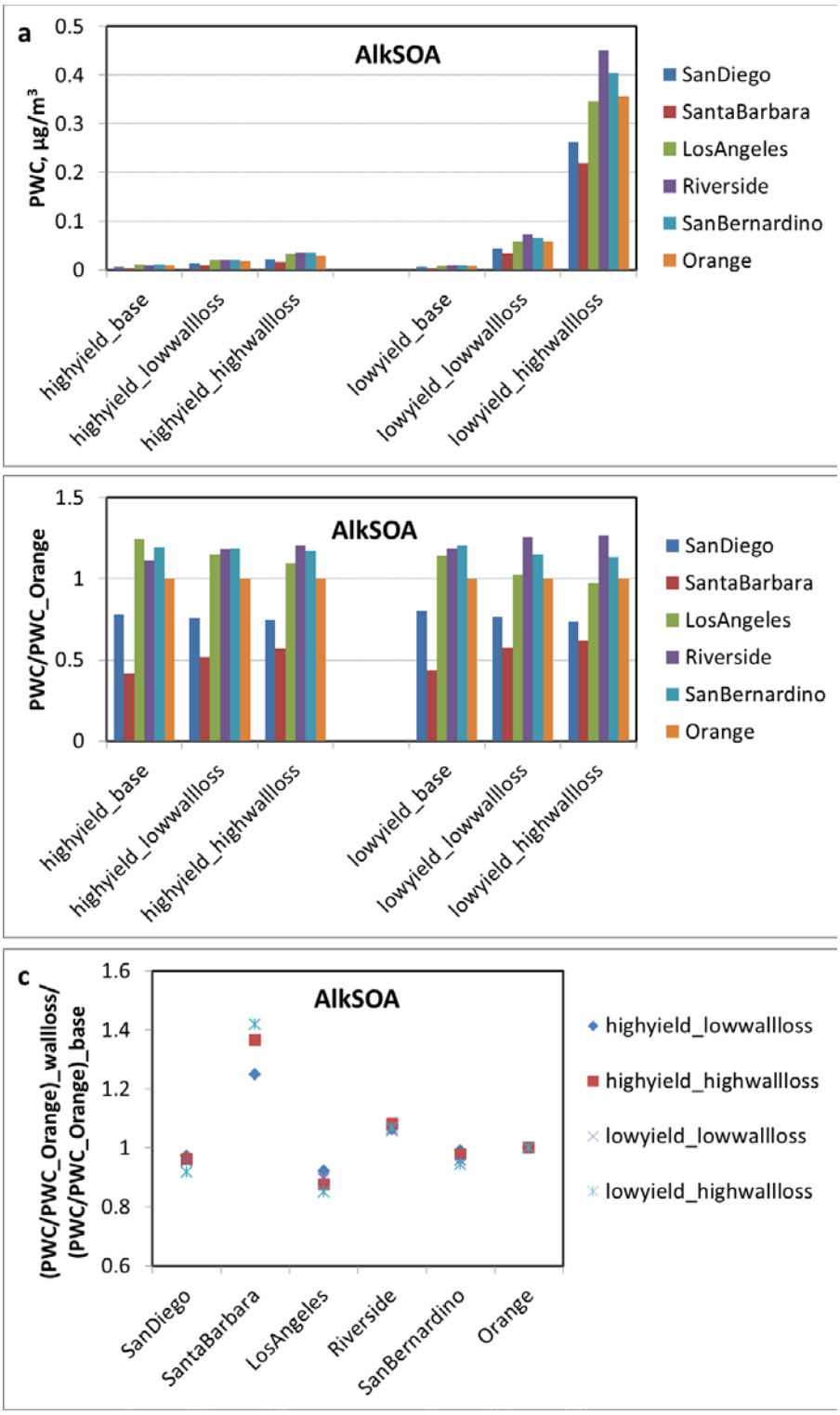

Figure S7 Same as Figure 9, but only for SOA derived from long alkanes (AlkSOA).

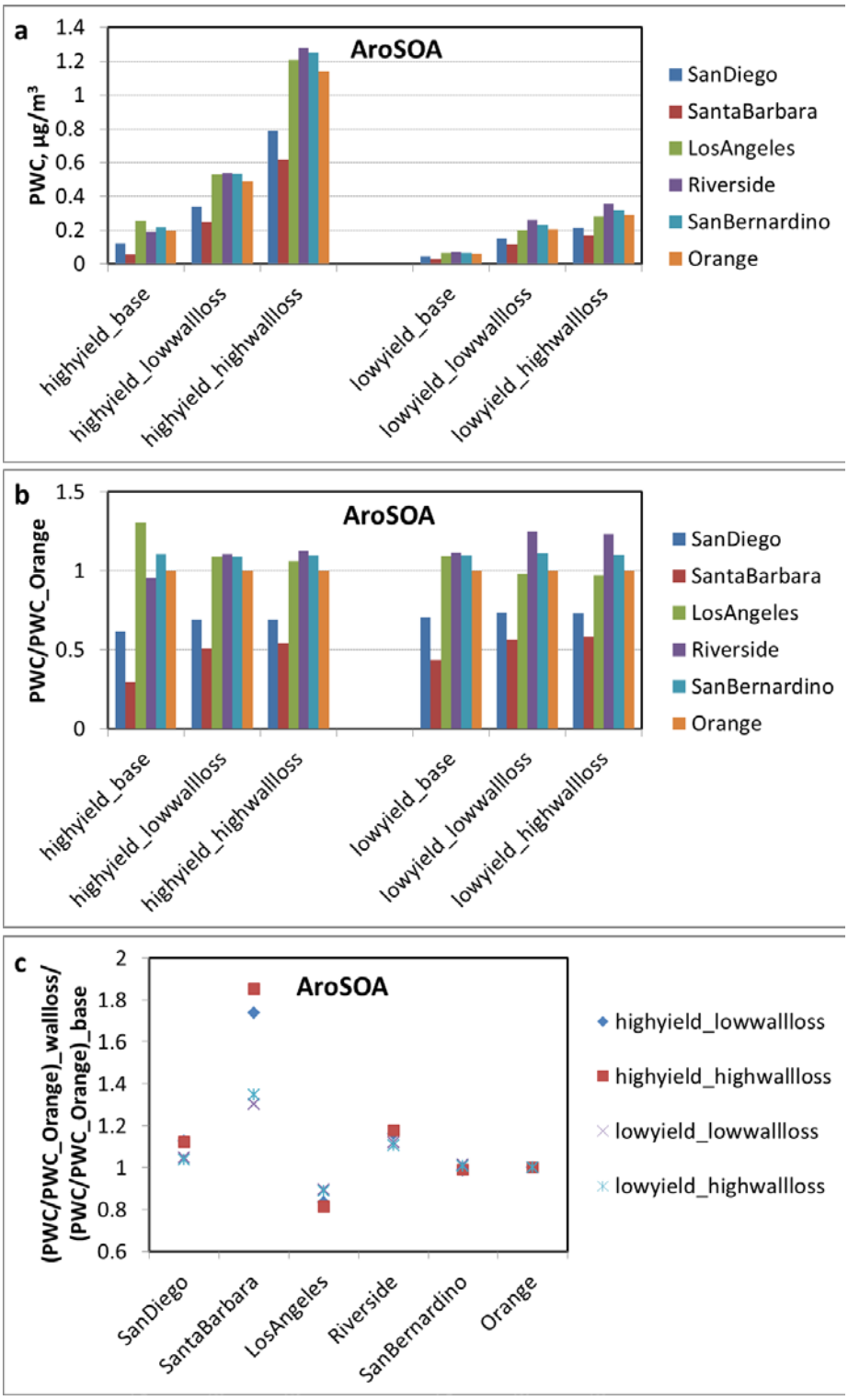

Figure S8. Same as Figure 9, but only for SOA derived from aromatics (AroSOA).

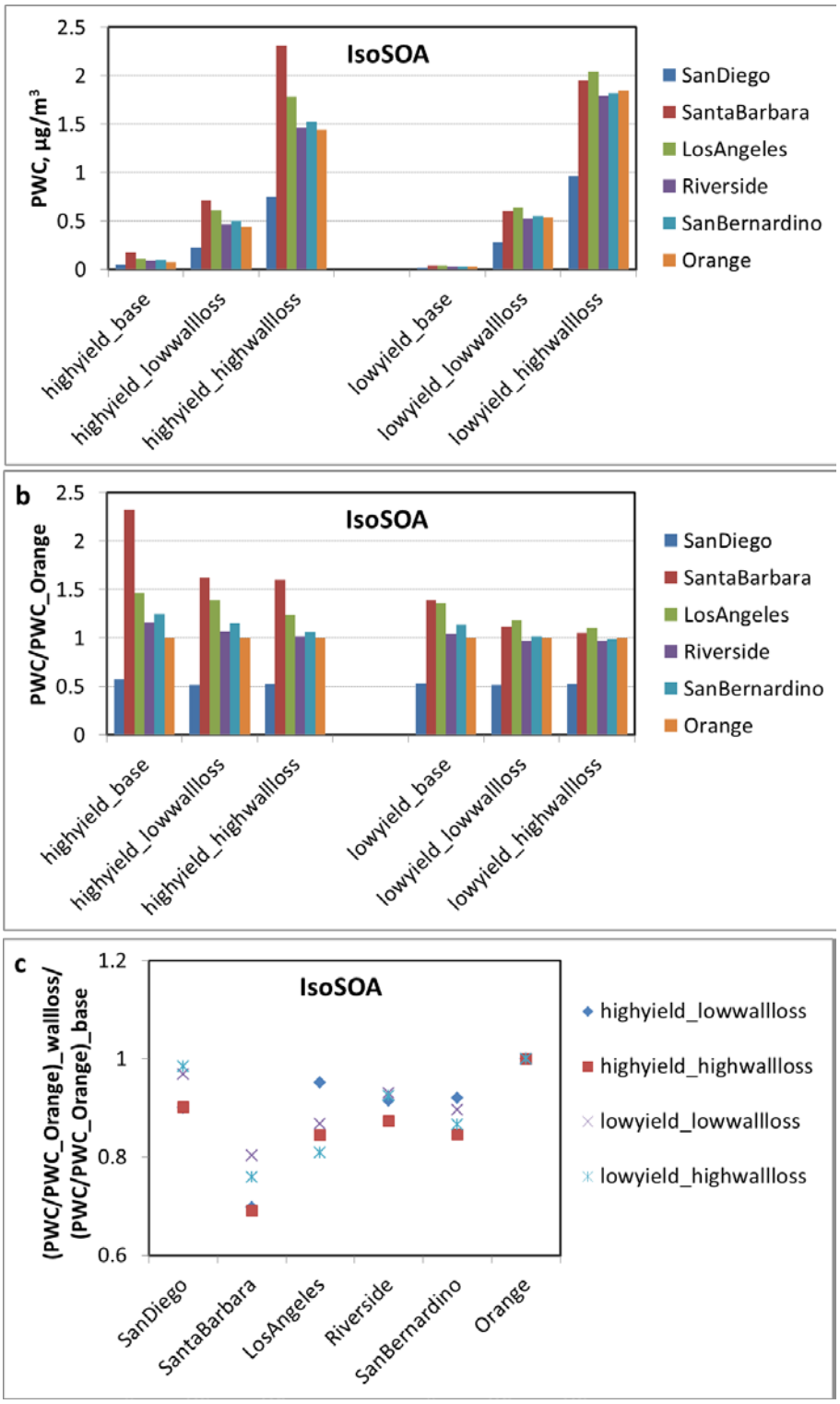

Figure S9. Same as Figure 9, but only for SOA derived from isoprene (IsoSOA).

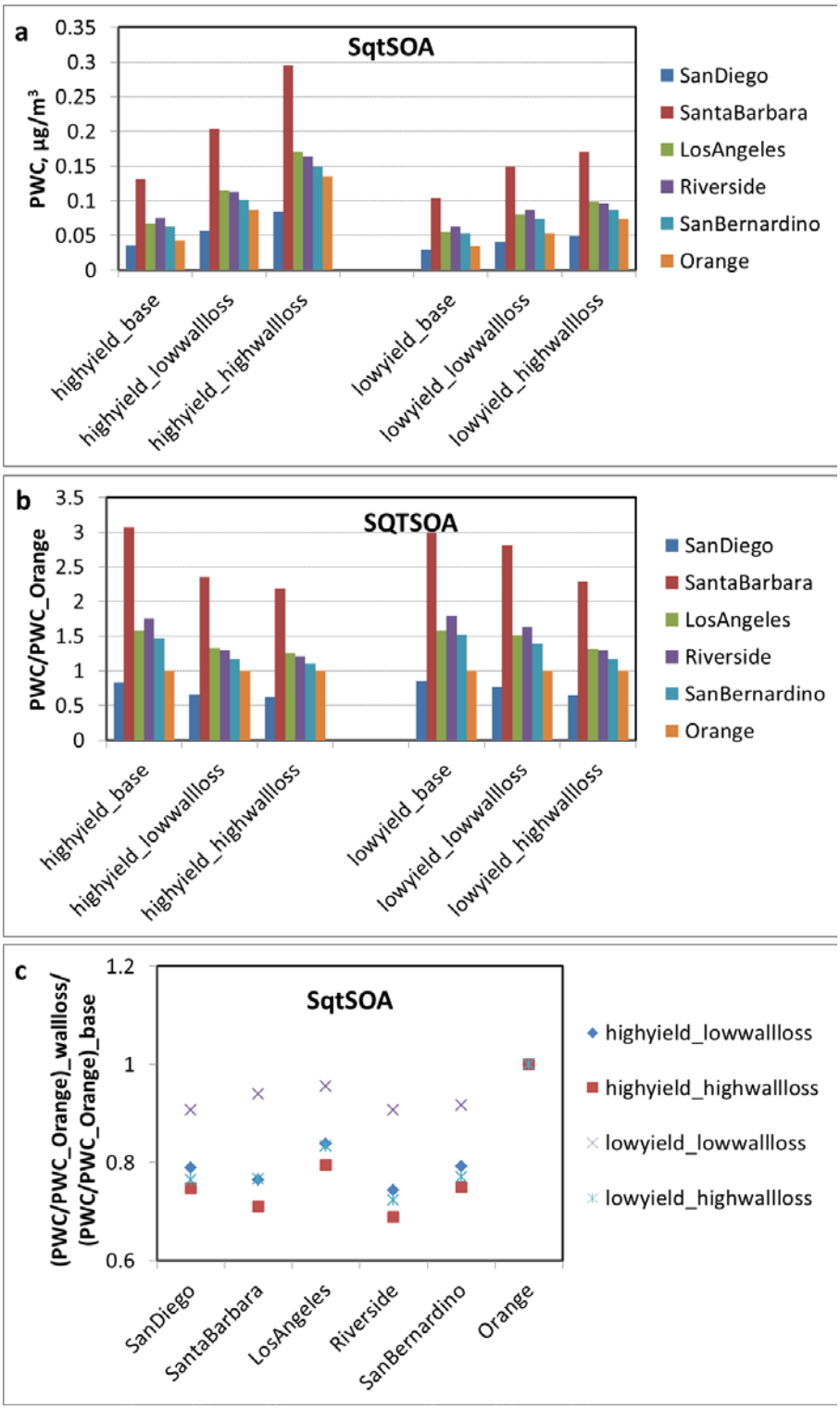

777

778 Figure S10. Same as Figure 9, but only for SOA derived from sesquiterpenes (SqtSOA).

779

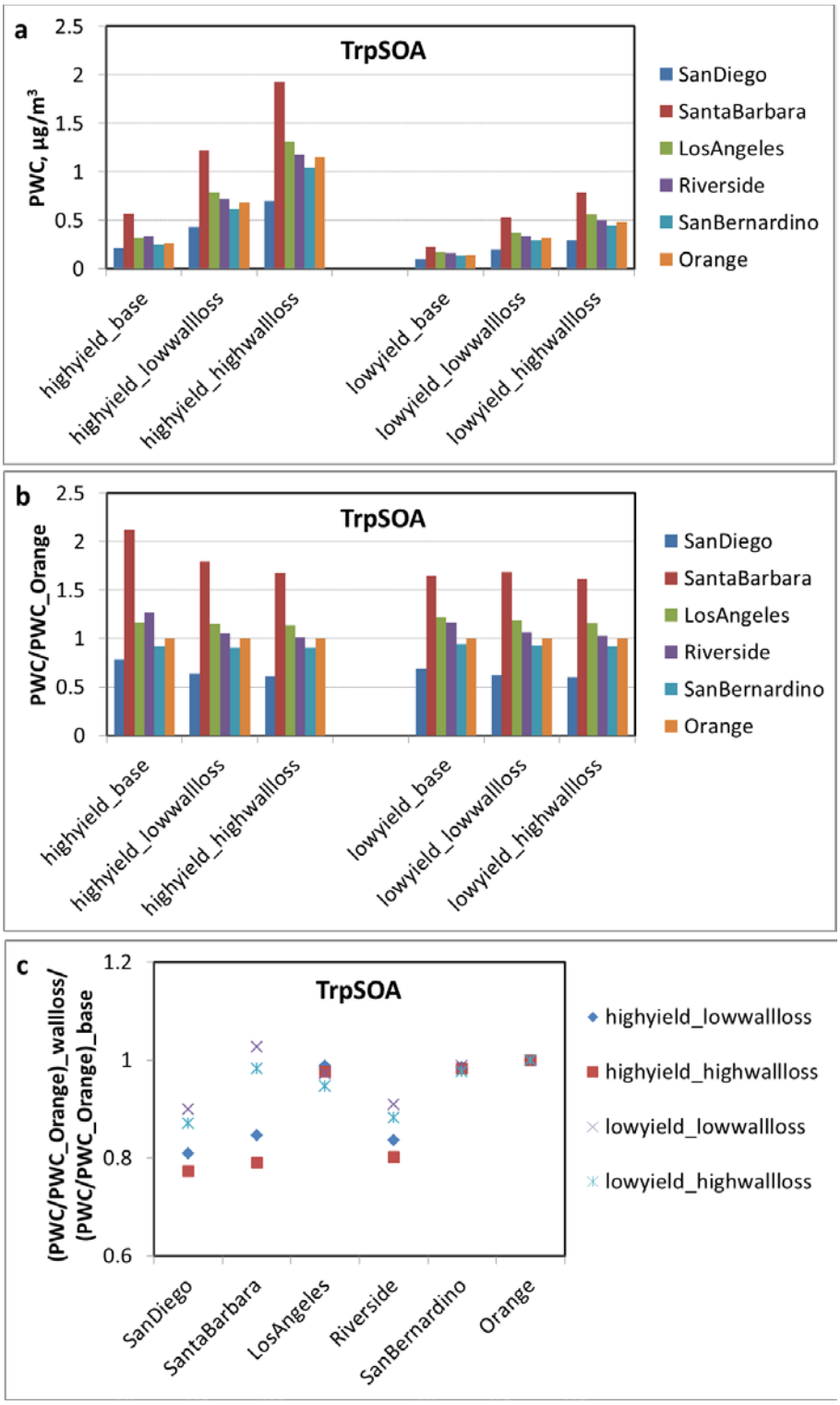

780

781 Figure S11. Same as Figure 9, but only for SOA derived from monoterpenes (TrpSOA).

782